SPECTRAL TECHNOLOGIES FOR ANALYZING 3D CONVERGING-DIVERGING NOZZLE, VENTURI TUBE, AND 90-DEGREE BEND DUCT

Undergraduate Honors Thesis

In Partial Fulfillment of the Requirements for
Graduation with Distinction and Honors in the
Department of Mechanical Engineering at
The Ohio State University

by

Rory C. Kennedy

Spring 2012

Advisor: Oliver G. McGee III, Ph.D. - Howard University, Washington, D.C.

This work was supported by the United Technologies Corporation and the Air Force Research Laboratory

Abstract

Computational fluid dynamics (CFD) is used to provide detailed predictions of complex fluid flows. CFD enables scientists and engineers to perform numerical experiments or computer simulations in a virtual flow laboratory. This study focuses on CFD for predicting the performance map of various Turbomachinery and nozzle configurations. The performance map can be characterized as the pressure ratio and efficiency of aircraft engines. Since small improvements in engine efficiency can lead to huge savings in fuel costs for a fleet of commercial aircraft, scientists and engineers are very interested in CFD tools that can give accurate quantitative predictions of engine performance maps without the need to run as many costly full scale wind tunnel tests. A three-dimensional (3D) spectral procedure has been developed to predict the flow solutions for the various nozzle configurations. The flow predictions have been charted against the evidence of well-established test data previously obtained in the literature. A spectral analysis procedure was formulated to reduce the governing coupled nonlinear parabolic partial differential equations to associated coupled nonlinear algebraic equations for the unsteady viscous compressible flow inside the geometry configurations. No conventional ordinary differential equations and associated time-marching techniques linked with finite element, volume, or differencing methodologies were needed. Favorable agreement is shown between the present 3D spectral method predictions and previously published 3D finite volume predictions of the transonic flow. The phenomenology of 3D spectral calculated secondary flow in the nozzles were traced and compared to that previously published in the literature. The favorable results obtained from the study shows clear evidence that the 3D spectral procedure developed can be an important tool in analyzing aircraft engines to improve performance efficiencies.

Acknowledgements

This thesis is a compilation of countless hours of work I have performed for the past three years. None of this would be possible without my advisor and mentor Professor Oliver McGee. I met him three years ago serendipitously and I have been working with him ever since. He brought me with him to NASA Glenn Research Center to assist him with his research during summers 2010 and 2011, and he also brought me to Washington D.C. for a quarter to work with him and alongside a couple of brilliant Howard University mechanical engineering students. Not only has he given me this amazing opportunity, but he has also helped me push myself in the classroom and in other career choices.

I would like to thank Dr. Rob Siston of Ohio State University, Dr. Scott Sawyer of Akron University, NASA Glenn Research Center Employees Mark Celestina and Rod Chima, and undergraduate engineering students of Howard University Rishi Jaglal and Michael Gallion for their assistance in helping me pull this all together.

I would also like to thank the Ohio State University's College of Engineering, Howard University's College of Engineering, and the Air Force Research Laboratory for funding the project for the past three years.

Lastly, I would like to give thanks to my parents Mark and Julie Kennedy for putting up with me for the last three years. They have given me tremendous support and without them, I wouldn't have been able to do this. Thank you Mom and Dad for everything.

Table of Contents

List of Figures

List of Tables

Chapter 1: Introduction

The goal of computational fluid dynamics (CFD) is to provide detailed predictions of complex fluid flows of all sorts. CFD enables scientists and engineers to perform numerical experiments or computer simulations in a virtual flow laboratory reducing costly full-scale tests. This thesis focuses on CFD for predicting the performance map of various nozzle and geometry configurations. The performance map can be characterized as the pressure ratio and efficiency of aircraft engines. Since small improvements in engine efficiency can lead to huge savings in fuel costs for a fleet of commercial aircraft, scientists and engineers are very interested in CFD tools that can give accurate quantitative predictions of engine performance maps [1]. In the early literature only qualitative comparisons were made against experimental Mach contours.

There are many reasons why performance predictions in the early literature were scarce. One reason is in the past, computers could not effectively calculate the efficiency and loss due to its high dependence on viscous effects, which requires high grid resolution for successful calculation [1]. Currently, computers that are capable of performing such calculations are widely available for CFD analysts. Another reason for the scarcity of performance predictions in the early literature is it was difficult to obtain experimental data due to the small components and high speeds needed for transonic turbomachinery tests. Now with advance measuring technologies and high speed wind tunnels available to scientists, accurate test data of various transonic systems is obtainable. The data is used to validate CFD methods in virtual laboratories. CFD predictions are now becoming widely available and provide useful information for scientists and engineers to help them develop and test full scale turbomachinery prototypes.

1.1 Methodologies

A three-dimensional spectral procedure (reduced ordered method (ROM) analysis) has been developed to predict the Navier-Stokes flow solutions of various transport systems. Specifically, the transport systems are modeled as a hydrodynamic continuum utilizing only nodal data to describe the arbitrary volume in which the 3D unsteady Navier-Stokes equations (Equations 1-5) were explicitly solved. A spectral analysis procedure was formulated to reduce the governing coupled nonlinear parabolic partial differential equations to associated coupled nonlinear algebraic equations for the unsteady viscous compressible flow. To achieve this, the flow was subjected to constraints imposed by an assumed hydrodynamic state field (i.e., density, axial, swirl, radial velocities, temperature, enthalpy, entropy, and conducted-heat) at each fluidic point comprised of mathematically complete, orthonormal polynomials in coupled space-time multiplied by generalized coefficients. The coefficients were determined by constraining the polynomial series to satisfy the governing partial differential equations, initial conditions, and boundary conditions of the transonic flow inside the transport systems. No conventional ordinary differential equations and associated time-marching techniques linked with finite element, volume or differencing methodologies were needed.

For solving the nonlinear 3D convection-diffusion problems of high Reynolds number, the ROM analysis is implemented on variable geometry configurations through sub-domain isoparametric mapping and generalized Fourier series approximation theory. The 3D Navier-Stokes equation system (NS5) solved, including continuity, three directional (radial, axial, tangential) momentum, and energy involving five (5) unknown fluidic properties (density, radial, axial, and tangential velocities, and temperature), are:

Continuity

$$\frac{d(\rho)}{dt}+\frac{d(\rho\, u)}{dx}+\frac{d(\rho\, v)}{dy}+\frac{d(\rho\, w)}{dz}=0 \tag{1}$$

Radial (*x*) Momentum

$$\rho\frac{d(u)}{dt}+\rho u\frac{d(u)}{dx}+\rho v\frac{d(u)}{dy}+\rho w\frac{d(u)}{dz}+\frac{dP}{dx}-\mu\left(\frac{d^2(u)}{dx^2}+\frac{d^2(u)}{dy^2}+\frac{d^2(u)}{dz^2}\right)=0 \tag{2}$$

Axial (*y*) Momentum

$$\rho\frac{d(v)}{dt}+\rho u\frac{d(v)}{dx}+\rho v\frac{d(v)}{dy}+\rho w\frac{d(v)}{dz}+\frac{dP}{dy}-\mu\left(\frac{d^2(v)}{dx^2}+\frac{d^2(v)}{dy^2}+\frac{d^2(v)}{dz^2}\right)=0 \tag{3}$$

Tangential (*z*) Momentum

$$\rho\frac{d(w)}{dt}+\rho u\frac{d(w)}{dx}+\rho v\frac{d(w)}{dy}+\rho w\frac{d(w)}{dz}+\frac{dP}{dz}-\mu\left(\frac{d^2(w)}{dx^2}+\frac{d^2(w)}{dy^2}+\frac{d^2(w)}{dz^2}\right)=0 \tag{4}$$

3D Energy

$$\rho\frac{d(CvT)}{dt}+\rho u\frac{d(CvT)}{dx}+\rho v\frac{d(CvT)}{dy}+\rho w\frac{d(CvT)}{dz}+P\nabla U-\kappa\left(\frac{d^2(T)}{dx^2}+\frac{d^2(T)}{dy^2}+\frac{d^2(T)}{dz^2}\right)-\Phi=0 \tag{5}$$

The pressure can be calculated from the equation of state:

$$P=\rho RT \tag{6}$$

The flow systems were subject to non-slip velocity conditions on all surfaces.

The 3D Navier-Stokes equation system (NS7) solved, includes the NS5 system with the energy equation substituted by two additional equations of enthalpy (*h*, internal energy plus thermal energy, *dh*, work), and entropy creation (*ds*, losses), plus an additional equation for heat conductivity involving eight (8) unknown fluidic properties (density, radial, axial, and tangential velocities, temperature, enthalpy (*h*, internal energy plus thermal energy, *dh*, work), entropy creation (*ds*), and added heat (*dQ*, effecting temperature distribution through heat conductivity):

Enthalpy

$$\rho\frac{d(h)}{dt}+\rho u\frac{d(h)}{dx}+\rho v\frac{d(h)}{dy}+\rho w\frac{d(h)}{dz}-\frac{dP}{dt}-\kappa\nabla^2T-\Theta-\mu(u\nabla^2u+v\nabla^2v+w\nabla^2w)=0 \qquad (7)$$

Entropy Creation

$$Tds-\kappa(\frac{d^2T}{dx^2}+\frac{d^2T}{dy^2}+\frac{d^2T}{dz^2})-\Theta=0 \qquad (8)$$

Heat Conductivity

$$dQ+\kappa(\frac{d^2T}{dx^2}+\frac{d^2T}{dy^2}+\frac{d^2T}{dz^2})=0 \qquad (9)$$

1.2 Purpose of Research

If reduced-ordered spectral technologies can be proved to find smooth, unique, and computationally exact solutions to 3D unsteady NS transport systems, CFD methodologies would be change forever. It would allow scientists to settle far reaching questions in fluids engineering and reactive transport sciences. For transonic flow simulations, spectral CFD methodologies would allow scientists and engineers to simulate real life conditions, including unsteady turbulence flow, in a virtual laboratory. This would save efforts and energy used towards testing full scale models in wind tunnels. Spectral technologies will also be able to find where all the loss mechanisms are inside nozzles and turbomachines, so that scientists have a better idea how to develop a new more efficient prototype. Spectral technologies will also be more accessible to the science community because of its solving nature and not having to use a super computer to obtain accurate results. The analyses can predict complex fluid flows in intricate nozzle and turbomachinery geometry configurations by using a single computer.

Chapter 2: Findings of Work Completed

In order to verify the effectiveness and accuracy of the spectral methods and theory described, a series of problems were examined. The findings produced herein summarize a number of theoretical problems of the associated literature as well as industry models, apropos to steady advection-diffusion, unsteady convection-diffusion, and unsteady compressible viscous flows. The three problems examined were a converging-diverging nozzle, a venturi tube, and a rectangular 90-degree bend duct. Each problem has different geometrical characteristics that determine how the flow properties will react as the fluid flows through the geometry. The three problems are rather simple compared to NASA test rotors; however, they all have geometry characteristics that are similar to NASA test rotors when all three problems are combined. If the ROM analysis can predict the flow properties of the three problems posed effectively and accurately, then the ROM analysis can be used to analyze NASA test rotors as well as other test rotors that exist in the literature.

2.1 Converging-Diverging Nozzle

Consider the 3D gradually converging-diverging industry nozzle (Figure 1) with given inlet conditions: $\rho_o = 0.6528\ kg/m^3$, $T_o = 249.15K$, $\mu = 1.79\text{x}10^{-5}$, $\kappa = 2.6\text{x}10^{-2}$, $\gamma = 1.4$. The cross section area distributions of the testing converging diverging nozzle: $A(x) = 1 - 0.8x(1-x)$, $0<x<1m$. When inlet Mach = 0.553 with equivalent Reynolds number, $Re = 6.4\text{x}10^6$, the flow Mach number will reaches one at throat area ($y = 0.5m$) and a shock will occurred at the diverging area. Flow passage discretization for the 3D model has 40 sub-domains with total $13\text{x}10^3$ points within the domain for the solutions.

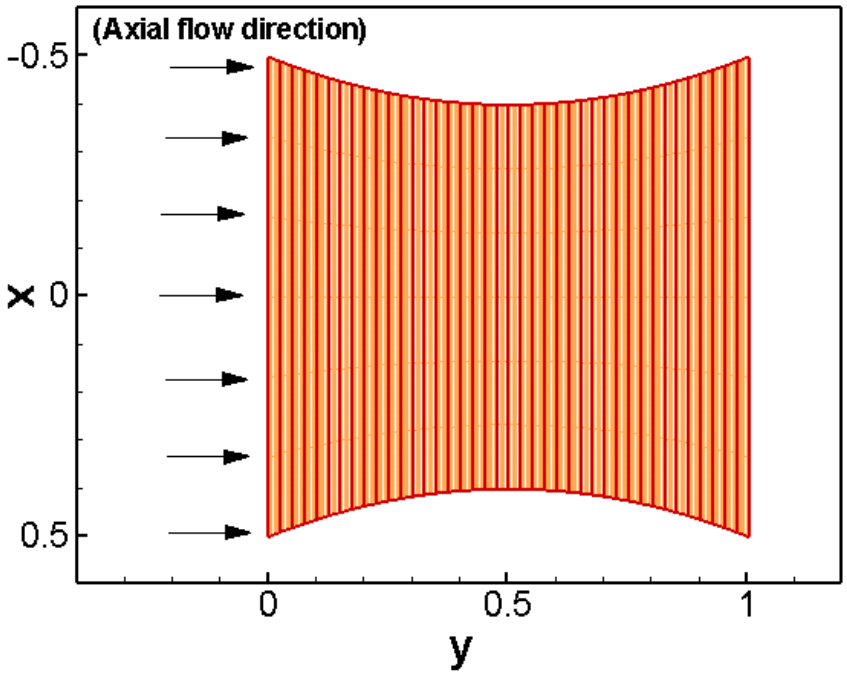

Figure 1: Converging-diverging industry nozzle.

Since the nozzle flow can be seen basically as one dimensional flow, 3D NS5 transonic and supersonic flow solutions for this gradually converging-diverging nozzle can be obtained and compare to one dimensional isentropic, entropic exact solutions [2] and pseudo-spectral & inviscid results [3]. Constant mass continuity in a gradually converging-diverging nozzle, which after differentiation and rearrangement, yields a sum of proportional changes in duct area, density, and axial Mach velocity. Driven largely by a ratio of proportional changes in duct area (dA/A) to axial velocity (du/u) [*i.e.*, $(dA/A)/(du/u) = -(1-M^2)$], Table 1 illustrates how changes in the fundamental transport flow equations (mass continuity and momentum) shifts flow quantities, such as axial velocity, pressure, density, temperature, and entropy in converging and diverging flows.

Table 1: Subsonic and supersonic flows in converging and diverging nozzles.

Geometry	**Converging**		**Diverging**	
Flow	Mach > 1	Mach < 1	Mach > 1	Mach < 1
Axial Velocity (*u*)	Decrease	Increase	Increase	Decrease
Pressure (*P*)	Increase	Decrease	Decrease	Increase
Density (ρ)	Increase	Decrease	Decrease	Increase
Temperature (*T*)	Increase	Decrease	Decrease	Increase
Entropy (*s*)	Constant	Constant	Constant	Constant

The subsonic, transonic and supersonic results are shown below in Figure 2Figure 7 clearly illustrate the findings of Table 1, before and after the shock, where *red, blue,* and *magenta* represent the solutions of exact one-dimensional isentropic flow, exact one-dimensional entropic [2], and 3D NS flow, respectively. Also, the pseudo-spectral & inviscid results [3] are shown on the right hand side of Figure 2. Velocity, density, temperature pressure, enthalpy, and entropy creation contours in the passage are also given below. For the gradually converging-diverging nozzle case study, the 3D NS analysis successfully obtained the steady-state flow solutions for the nozzle subsonic and transonic flow in the converging area, becoming supersonic in the diverging region, and capturing the shock discontinuity at approximately $x = 0.8m$. From the comparisons, one can see that the 3D NS5 and 3D NS8 findings are in very good agreement with the exact isentropic and entropic solutions along with Hanley [3] pseudo-spectral computations and inviscid theory findings. Across the board, the calculation of the entropy creation, *ds*, as well as, the entropy generation rate, *dS/dt*, in the nozzles, was a relatively easy task, once the velocity and temperature fields are known in detail. The global entropy generation rate was directly related to the overall losses (or efficiency), but its functional dependence on the local characteristics of the flow field was not immediately detectable. On the contrary, knowledge of the local entropy creation or entropy generation rate at each point in the nozzle

provided immediate useful insight into the relative importance of the different sources of irreversibility across the nozzle's NS transport processes.

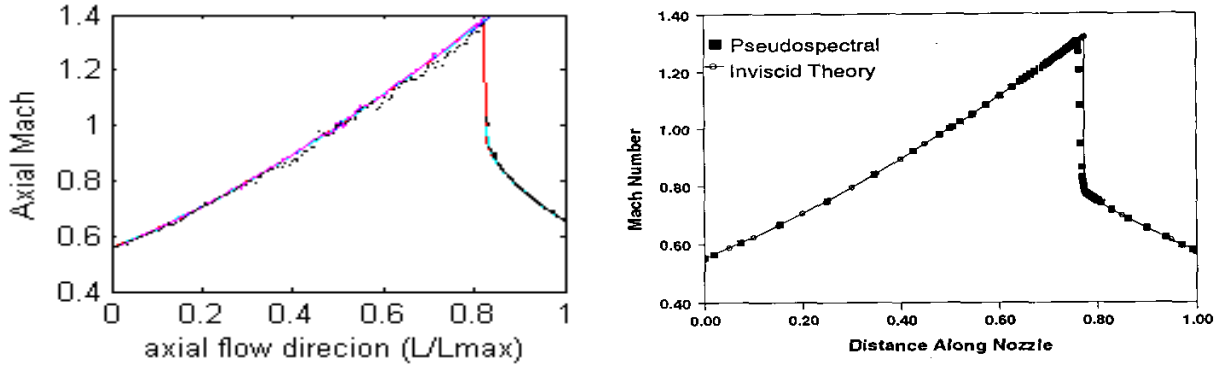

Figure 2: Findings of transonic and supersonic transport axial Mach flow across a gradually converging-diverging nozzle, comparing exact 1-D isentropic (shown in red), exact 1-D entropic (shown in blue) [2], 3D NS5 (shown in magenta), and 3D NS8 (shown in black)) with published findings of Hanley [3], comparing a pseudo-spectral computational transport analysis with an inviscid transport theory (right).

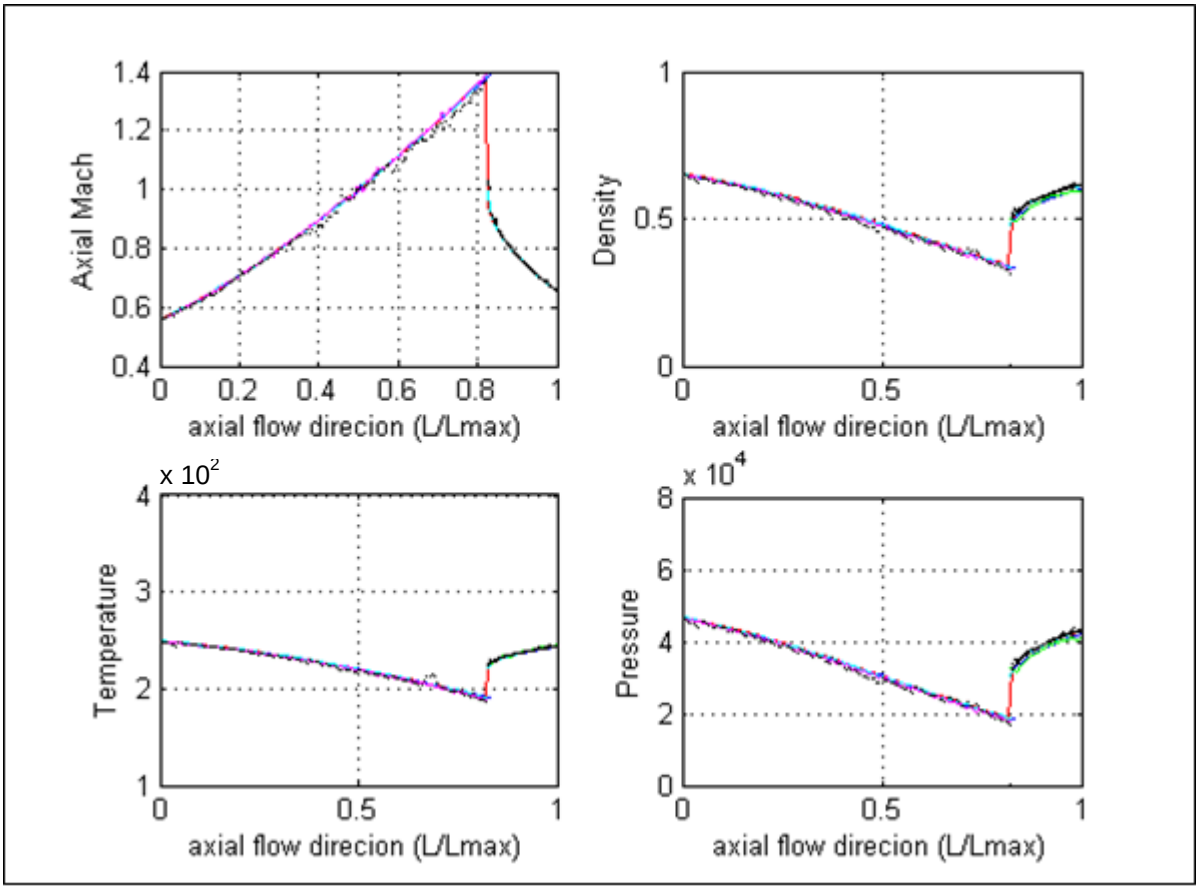

Figure 3: Findings of transonic and supersonic transport flow properties (axial Mach, density, temperature, and pressure) across a gradually converging-diverging nozzle, comparing exact 1-D isentropic (shown in red), exact 1-D entropic (shown in blue), 3D NS5 (shown in magenta), and 3D NS8 (shown in black).

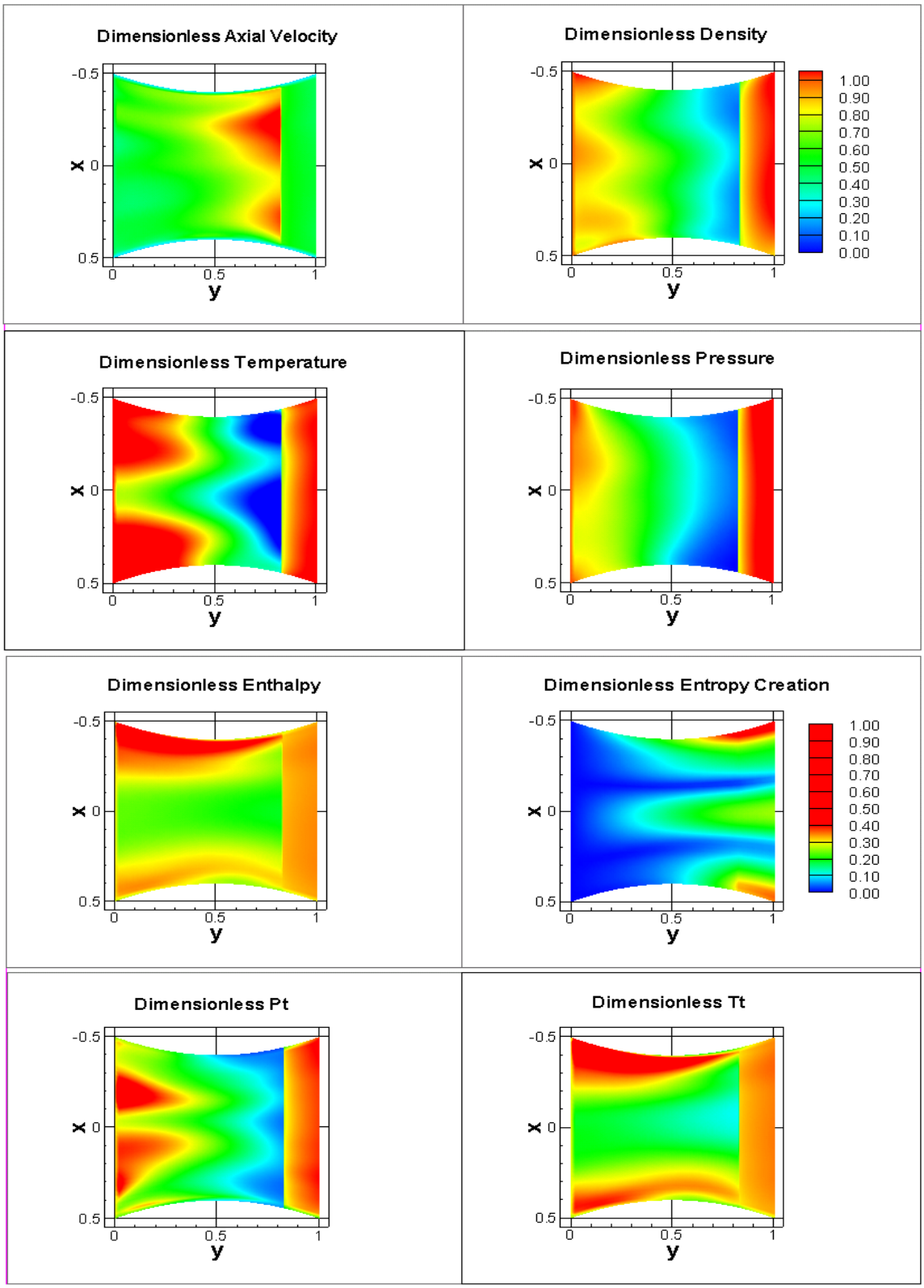

Figure 4: Results of 3D NS5 steady-state conservative transonic-supersonic flow solutions computed using Legendre non-periodic spectral approximations using 220 terms for each flow state (density, fluidic velocity (u,v,w), and temperature) incorporating 40,000 points in passage. Results are normalized to the maximum non-dimensional values.

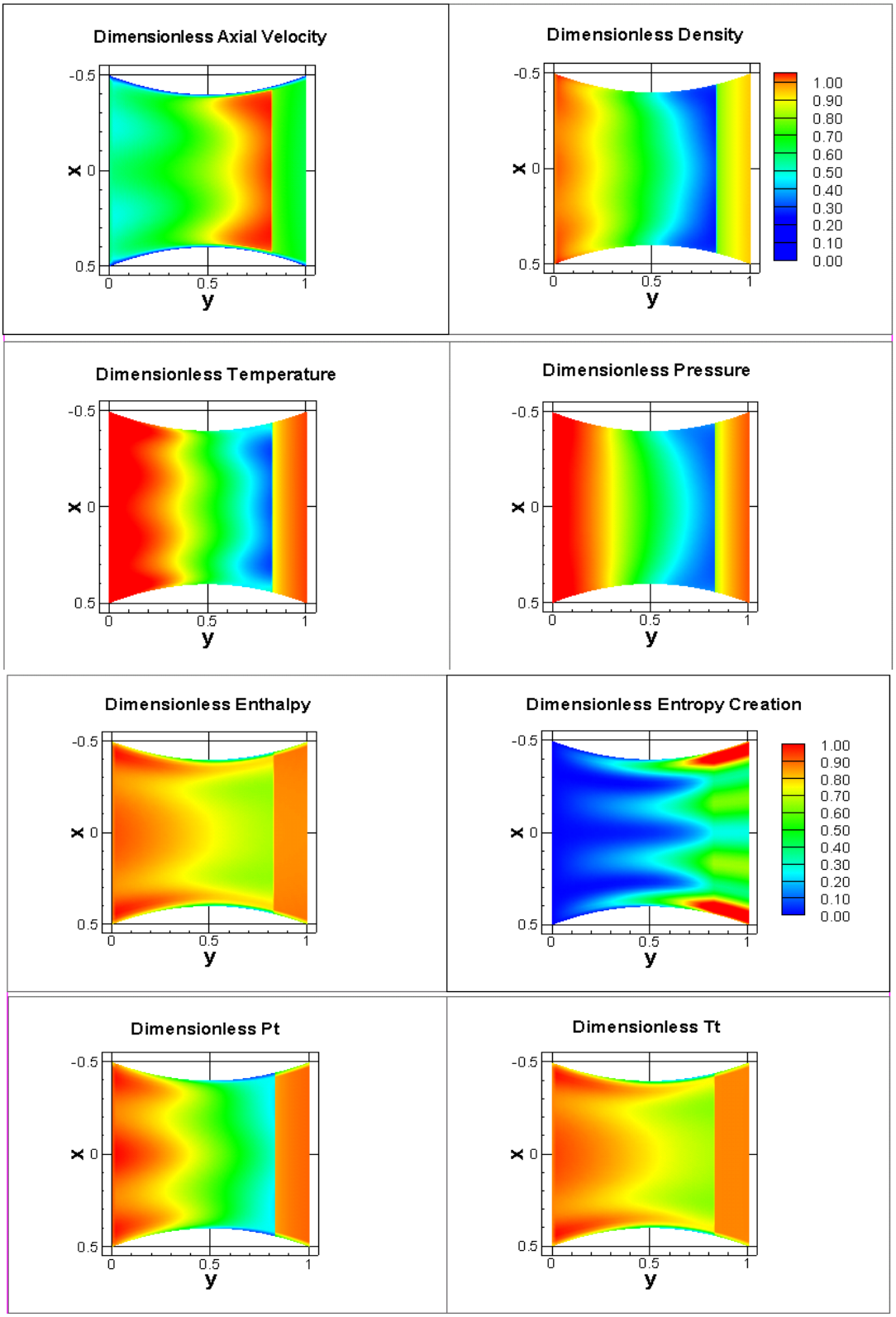

Figure 5: Results of 3D NS8 steady-state conservative transonic-supersonic flow solutions computed using Legendre non-periodic spectral approximations using 220 terms for each flow state (density, fluidic velocity (u,v,w), and temperature) incorporating 40,000 points in passage. Results are normalized to the maximum non-dimensional values.

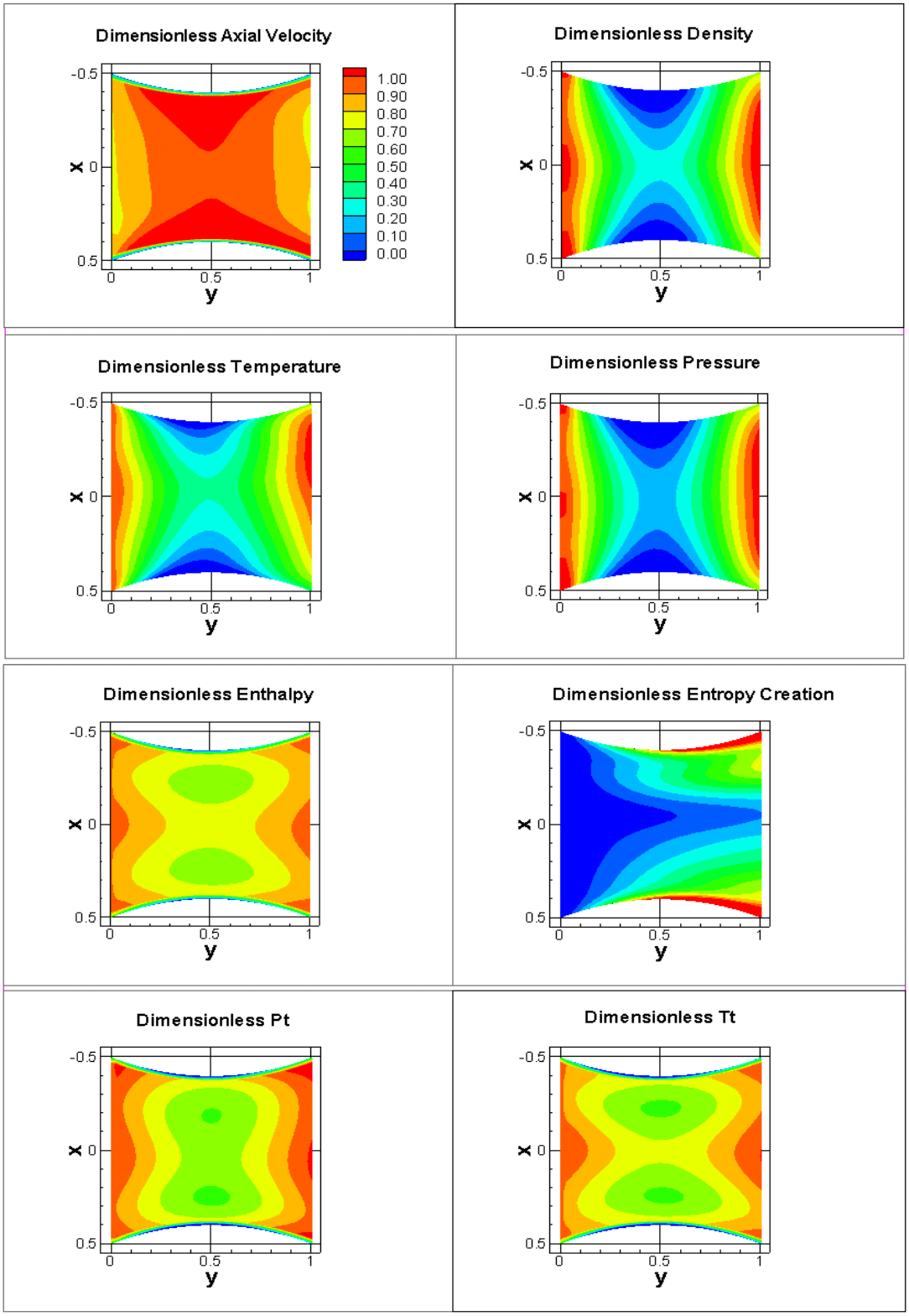

Figure 6: Results of 3D NS5 steady-state conservative subsonic flow solutions computed using Legendre non-periodic spectral approximations using 286 terms for each flow state (density, fluidic velocity (u,v,w), and temperature) incorporating 64,000 points in passage. Results are normalized to the maximum non-dimensional values of ideal isentropic solution: Mach: 0.39; density: 0.65; temperature: 249; pressure: 4.7e+4; enthalpy (h): 2.5e+5; entropy creation (dS): 260.

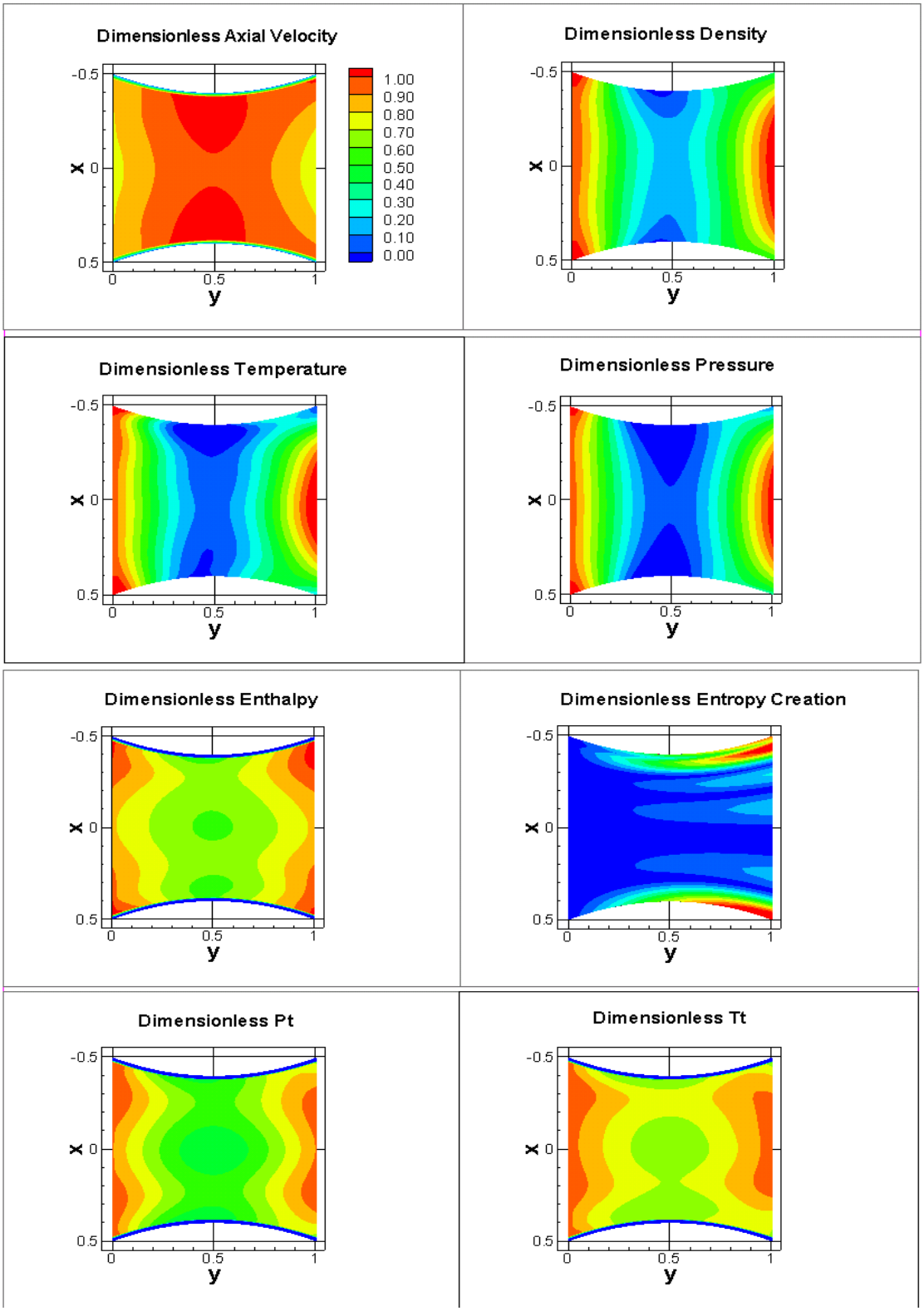

Figure 7: Results of 3D NS8 steady-state conservative subsonic flow solutions computed using Legendre non-periodic spectral approximations using 286 terms for each flow state (density, fluidic velocity (u,v,w), and temperature) incorporating 64,000 points in passage. Results are normalized to the maximum non-dimensional values of ideal isentropic solution: Mach: 0.39; density: 0.65; temperature: 249; pressure: 4.7e+4; enthalpy (h): 2.5e+5; entropy creation (dS): 260.

The same 3D gradually converging-diverging industry nozzle was also analyzed at subsonic speeds with given inlet conditions: $\rho_o = 0.6528\ kg/m^3$, $T_o = 249.15K$, $\mu = 1.79x10^{-5}$, $\kappa = 2.6x10^{-2}$, $\gamma = 1.4$. When inlet Mach = 0.30 with equivalent Reynolds number, $Re = 3.7x10^6$, the flow Mach number will never reach one and no shocks will occurred at the diverging area. The computation physical grid (x y z) composed of 64,000 points used for the subsonic analysis is shown in Figure 8 and the computational grid ($\xi\ \eta\ \zeta$) is shown in Figure 9.

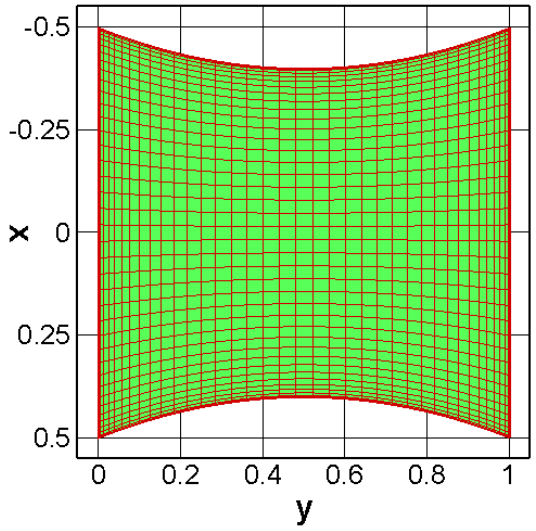

Figure 8: Computational and physical Chebyshev grids of a gradually converging-diverging nozzle for 3D NS5/NS8 analyses. Physical grid (x y z) = (40 × 40 × 40) points.

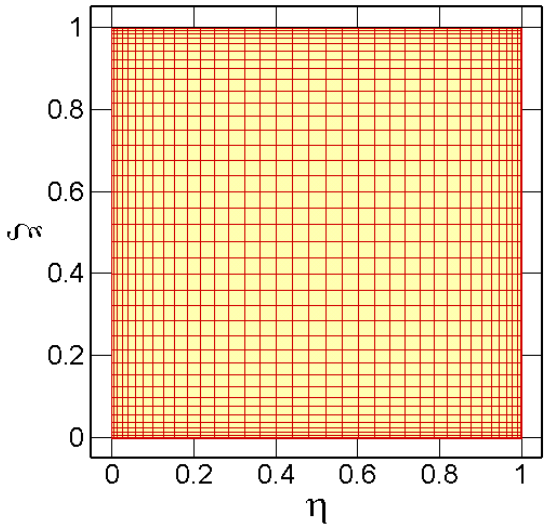

Figure 9: **Computational grid ($\xi \times \eta \times \zeta$) = (40 × 40 × 40) points.**

The results of the 3D NS5 steady-state conservative subsonic flow solutions computed using Chebyshev non-periodic spectral approximations for the subsonic gradually converging-diverging nozzle are shown in Figure 10Figure 11. A sensitivity analysis is shown in Figure 12. More sensitivity analyses of different solution sizes are shown in Appendix A. The sensitivities of each flow solution were overlaid on all twelve graphical comparisons. Table 2 displays the dependent variable sensitivities that were used during these analyses. Equations 10-11 show how the impulse stress and the entropy creation dependent variables were found. Equations 12-13 were the sensitivities used to show the flow choking relations inside the nozzle.

Table 2: Dependent variables sensitivities used during analyses.

Mach	Velocity (U,V,W)	Static Density	Static Pressure	Static Temperature	Impulse Stress	Entropy Creation	Total Pressure	Total Temperature
$\frac{dM^2}{M^2}$	$\frac{dV}{V}$	$\frac{d\rho}{\rho}$	$\frac{dp}{p}$	$\frac{dT}{T}$	$\frac{d\sigma}{\sigma}$	$\frac{d\bar{s}}{c_p}$	$\frac{dp_0}{p_0}$	$\frac{dT_0}{T_0}$

Impulse Stress

$$\frac{d\sigma}{\sigma} = \frac{d\kappa}{\kappa} + 2\left(\frac{dp}{p} + \frac{dM}{M}\right) \tag{10}$$

Entropy Creation

$$\frac{ds}{C_p} = \frac{dT_0}{T_0} - \left(\frac{\kappa-1}{\kappa}\right)\frac{dp_0}{p_0} \tag{11}$$

G Function and G-bar

$$(1-M^2)\frac{d(\text{'dependent variable'})/(\text{'dependent variable'})}{dy} = \bar{G}(y) = \frac{G(y)}{M^2} \tag{12}$$

G Function Elasticity

$$\frac{d(\bar{G})}{dy} = G\ Elasticity \tag{13}$$

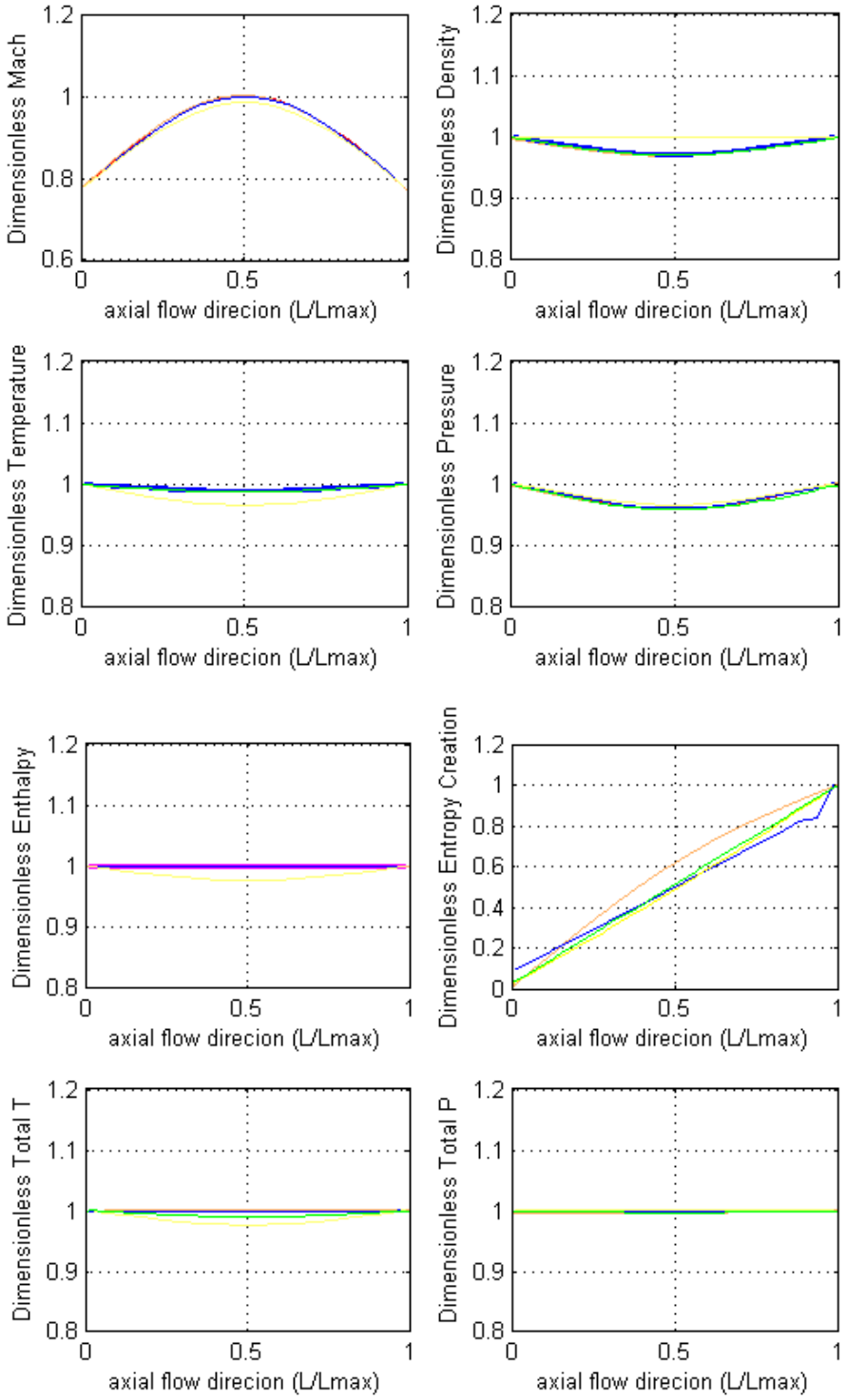

Figure 10: Gradually Converging-Diverging subsonic flow nozzle Quasi 3D and 3D Steady-state solutions. (Red: Exact 1-D isentropic solutions; Orange: Exact 1-D entropic solutions; Blue: Quasi 3D NS3 solutions; Pink: Quasi 3D NS6 solutions; Green: 3D NS8 solutions). The Quasi 3D steady-state conservative subsonic flow solutions computed using Chebyshev 20th order non-periodic spectral approximations using 20 points in the passage with polynomials for each flow state (density, axial velocity (v), temperature, enthalpy, entropy, and heat transfer).

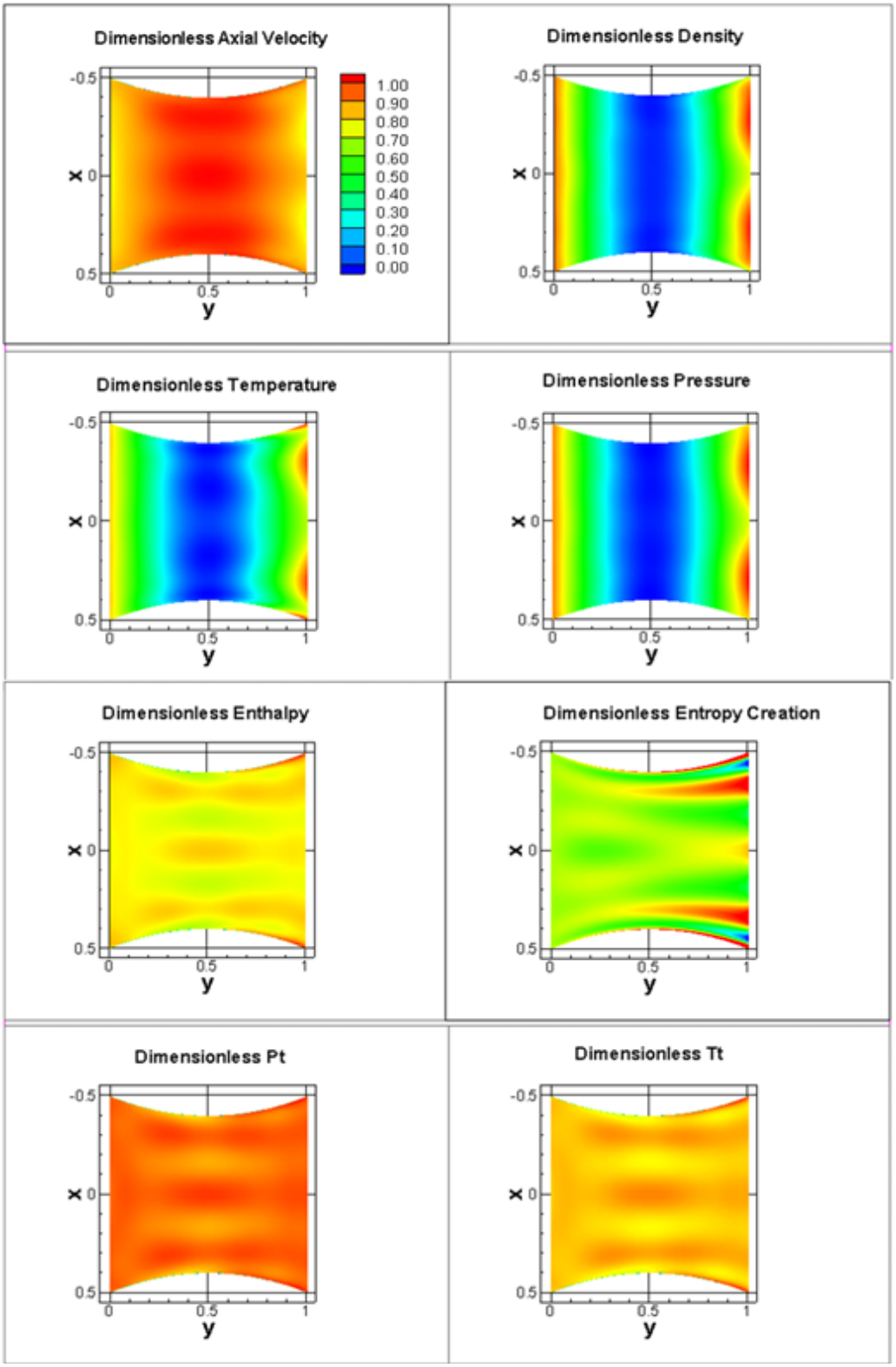

Figure 11: Results of 3D NS8 steady-state conservative subsonic flow solutions computed using Chebyshev non-periodic spectral approximations using 286 terms for each flow state (density, fluidic velocity (u,v,w), and temperature, enthalpy, entropy, and heat transfer) incorporating 64,000 points in passage. Results are normalized to the maximum non-dimensional values of ideal isentropic solution: Mach: 0.39; density: 0.65; temperature: 249; pressure: 4.7e+4; enthalpy (h): 2.5e+5; entropy creation (dS): 260.

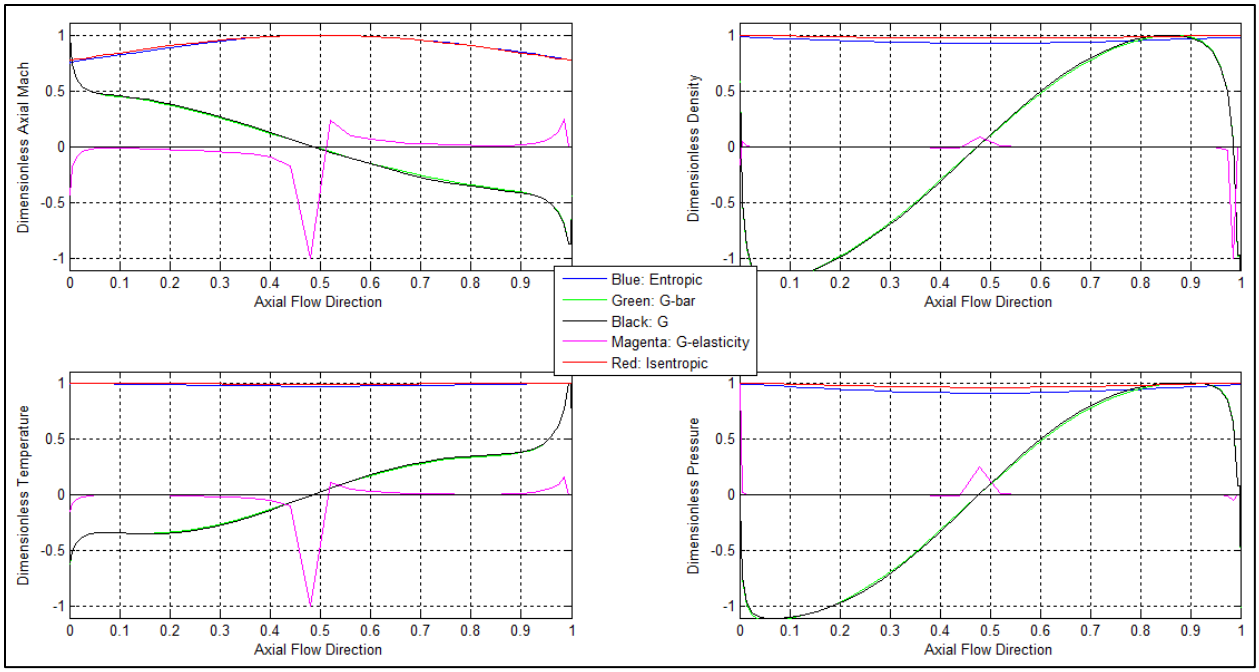

Figure 12: Sensitivities of 3D NS5 steady-state conservative subsonic flow solutions using Chebyshev non-periodic spectral approximations using 286 terms for each flow state (density, fluidic velocity (u,v,w), and temperature) incorporating 64,000 points in passage. Results are normalized to the maximum non-dimensional values of the 3D NS5 solutions.

2.2 Venturi Tube

The second problem examined was venturi tube idealized as a 3D converging-diverging nozzle, which introduces subsonic, transonic, and supersonic transport flow phenomena including viscous boundary layer effects in a 3D unsteady NS analysis. Consider the 3D converging-diverging industry nozzle shown in Figure 13 with given inlet conditions: $T_o=2(10^3)$ K, $P_o=10$ atm. Mach number reaches unity at the throat area (y=0) with equivalent Reynolds number Re = $3(10^7)$. A representative spectral idealization of the flow passage employed is shown in Figure 14, which incorporates 40 sub-domains with a total $40(16^3)$ points used to capture details of the unsteady, viscous transport flow processes.

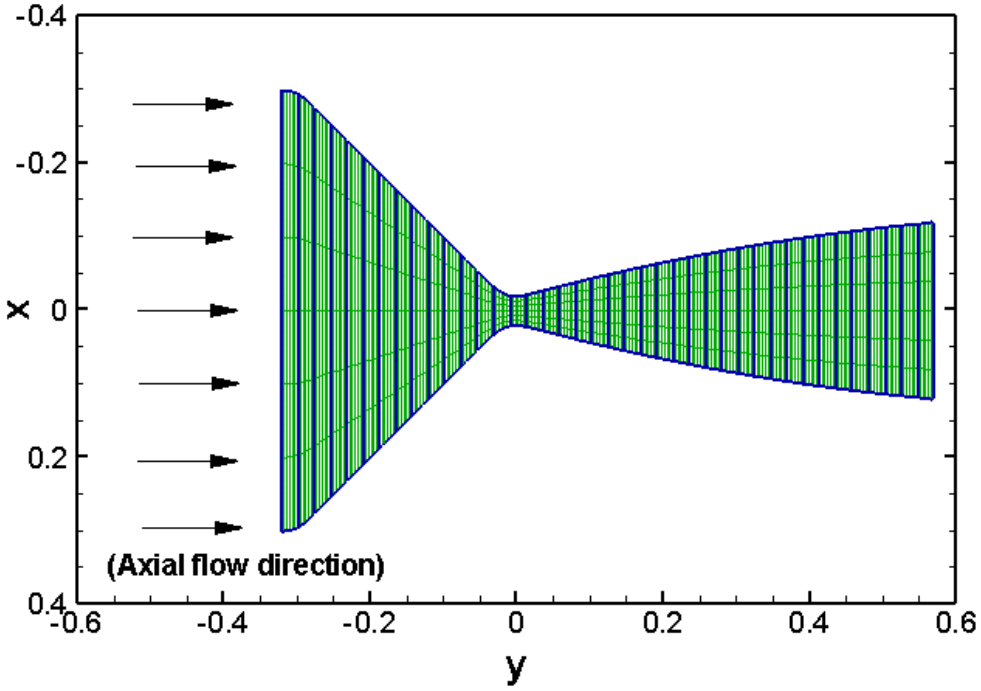

Figure 13: Uniform physical grid (Legendre non-periodic computational approximation) of the 3D venturi tube industry nozzle.

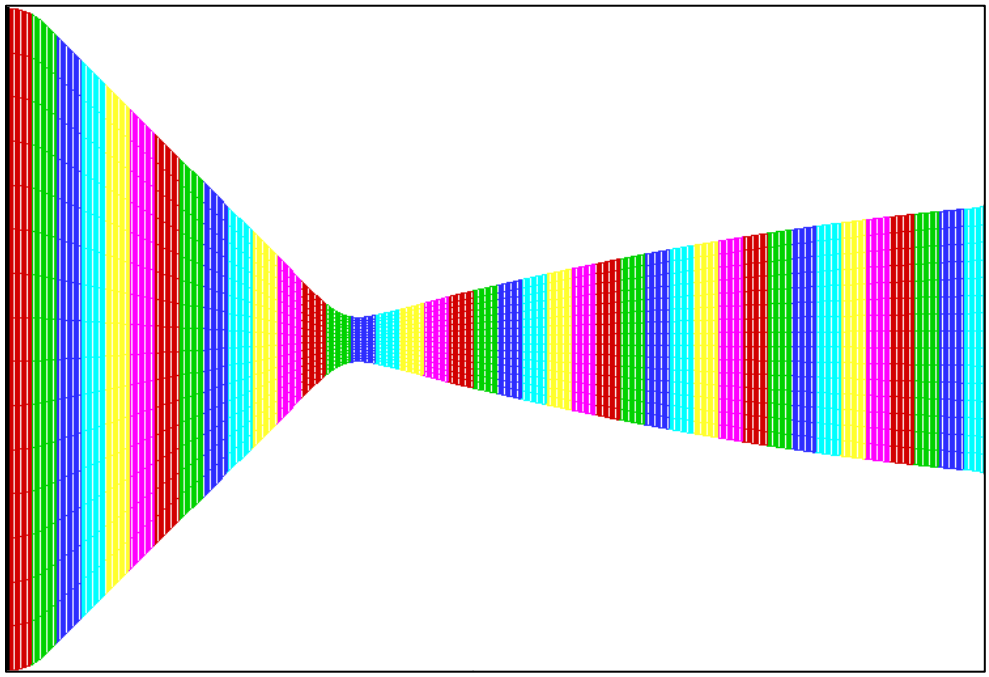

Figure 14: Uniform physical grid (Legendre non-periodic computational approximation) of the 3D venturi tube industry nozzle with 40 sub-domains denoted by color. Each sub-domain has 4,096 points (16x16x16 xyz) for a total of 163,840 points through the nozzle passage

Steady state findings of transonic and supersonic transport flow solutions are shown in Figure 15, where red, blue, and magenta colored data coinciding therein represent the solutions of exact 1D isentropic, exact 1D entropic and unsteady 3D NS5 and 3D NS8 solutions, respectively. The 3D NS solutions are transonic and supersonic flow of high Reynolds number on the order of 10^7. The 3D NS solutions agree favorably with the exact isentropic and entropic solutions. The results show the axial velocity in the nozzle accelerates past the Mach number of unity at the throat area and gradually increases to supersonic Mach number well over 3 at the outlet. Details of the 3D NS flow processes are summarized in the axial Mach, velocity, density, temperature, and pressure contours through the nozzle passage shown in Appendix B. These contours depict fundamentally not only how axial Mach velocity increases significantly and consistently with density, temperature, and pressure drop across the nozzle passage, but also how viscous boundary layer effects develop, and how convective heat transfer, that occurs between the nozzle wall surface and the flowing fluid over it, advances particularly in the supersonic diverging regions of the nozzle passage. The thermal effects of the nozzle surfaces on the flowing fluid, like the viscous effects, are confined to a region near the surface that is thin compared to the characteristic length of the nozzle surface, given the high Reynolds number on the order of 10^7 treated in this industry nozzle case study. Generally speaking, the boundary layer thickness relative to the characteristic length of the nozzle is at most proportional to the order of $(Re)^{-1/2} = (10)^{-7/2}$. In most of the components of such gas nozzle transport systems, analysts aim to minimize viscous effects, working to achieve such high Reynolds numbers and thin boundary layers, as predicted in Figure 16.

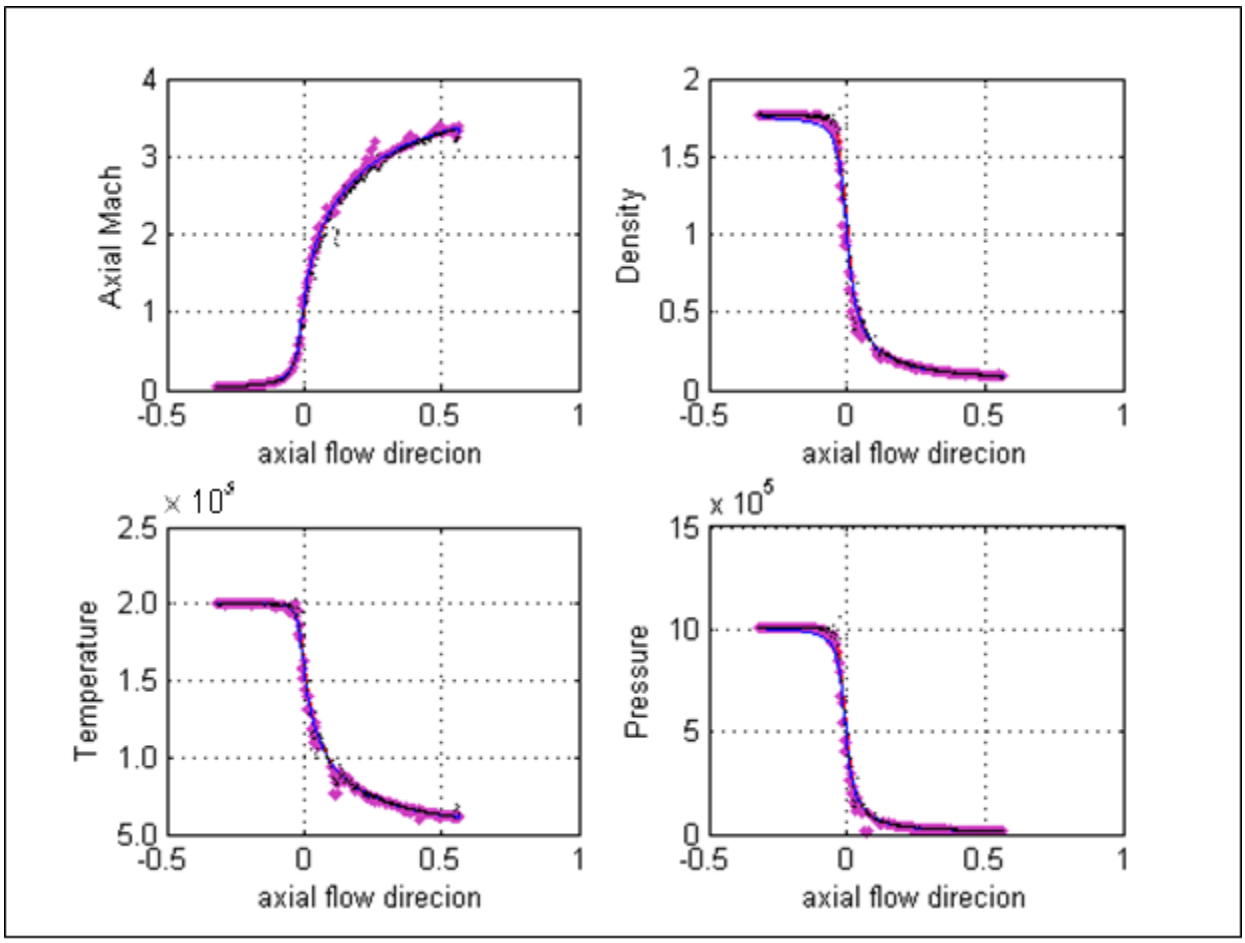

Figure 15: Steady state findings of transonic and supersonic transport flow properties (axial Mach, density, temperature, and pressure) across a gradually converging-diverging industry nozzle, comparing exact 1D isentropic (shown in *red*), exact 1D entropic (shown in *blue*), 3D NS5 Legendre non-periodic spectral calculation (shown in *magenta*), and 3D NS8 Legendre non-periodic spectral calculation (shown in *black*) solutions.

A sensitivity analysis of the 3D NS8 steady-state conservative transonic flow solutions computed using Legendre non-periodic spectral approximations is shown in Figure 16. The sensitivities of each flow solution were overlaid on all twelve graphical comparisons. One run was examined for the converging-diverging venturi tube industry nozzle. The run incorporated 40 sub-domains of 4,096 points each (16x16x16, xyz) for a total grid size of 163,840 points in the flow passage using 192 terms for each flow state (density, fluidic velocities (u,v,w), and temperature, 960 total terms). Inlet conditions were as follows: Mach: 0.0384; ρ_o=1.765 kg/m^3; T_o=2000K; μ=1.79x10^{-5}; κ=2.6x10^{-2}; γ=1.4; *Re* = 2.182x10^7.

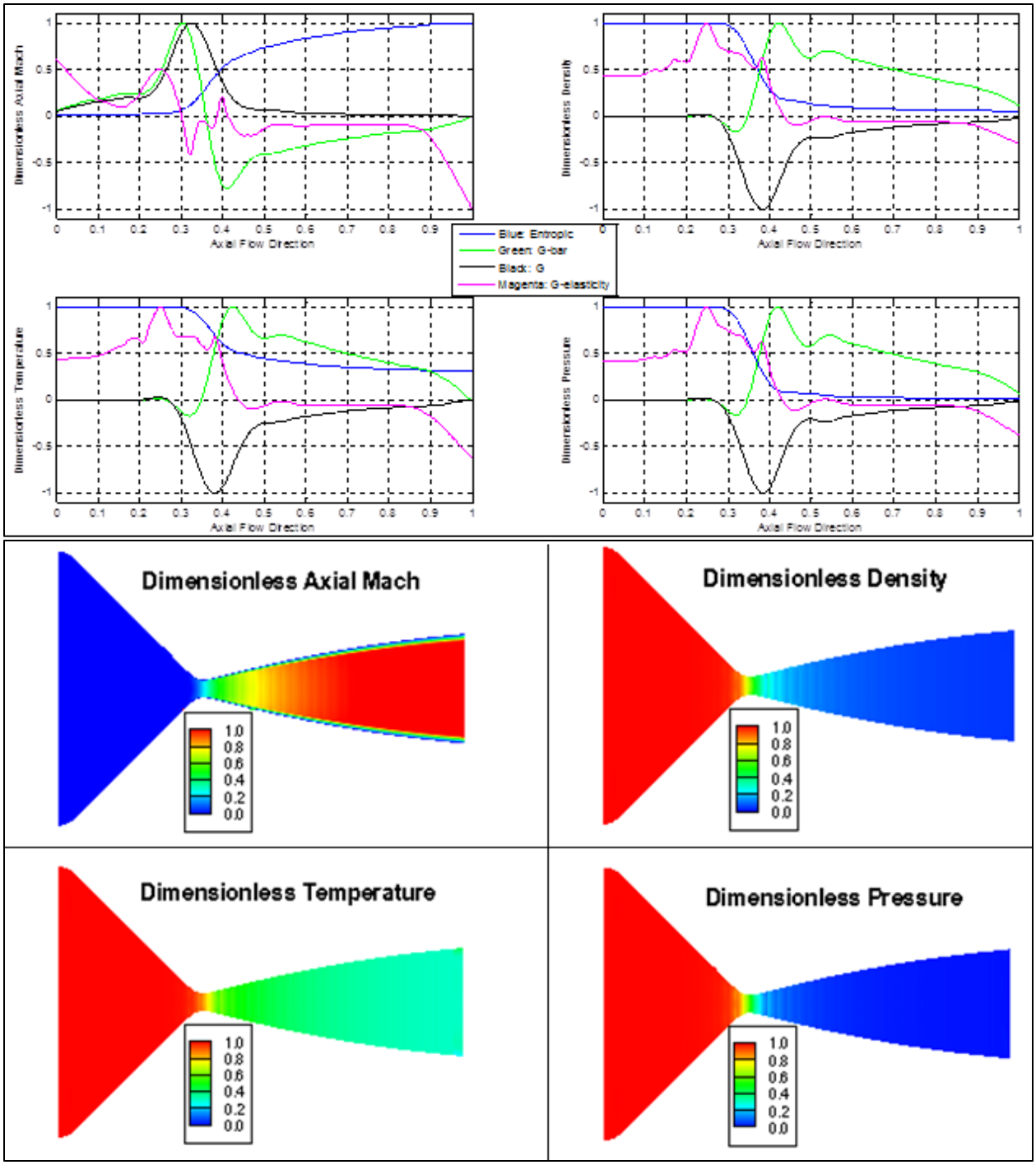

Figure 16: Results of 3D NS8 steady-state conservative transonic and supersonic flow solutions computed along with the sensitivities using Legendre non-periodic spectral approximations using 192 terms for each flow state (density, fluidic velocity (u,v,w), and temperature, 960 total terms) incorporating 163,840 points in passage. Results are normalized to the maximum non-dimensional values of the 3D NS8 solutions; the 3D NS8 loss sensitivity measures for the run was also examined, and are normalized to the maximum non-dimensional values of the G-stress and G-entropy.

2.3 Rectangular 90-Degree Bend Duct

To further verify the effectiveness and accuracy of the spectral methods and theory described, another problem was examined. Warren Joy's thesis *Experimental Investigation of Shear Flow in Rectangular Bends* [4] investigated the secondary circulation phenomenon that exists downstream from when fluid flow is forced around a bend. One experimental test Joy performed included a test setup of a 90 degree bend, rectangular cross section 5 by 10 inches, with a bend radius of 15 inches (Figure 17). A velocity gradient of air was introduced to the structure and was forced around the bend while velocity and pressure measurements were recorded at various stations inside the structure.

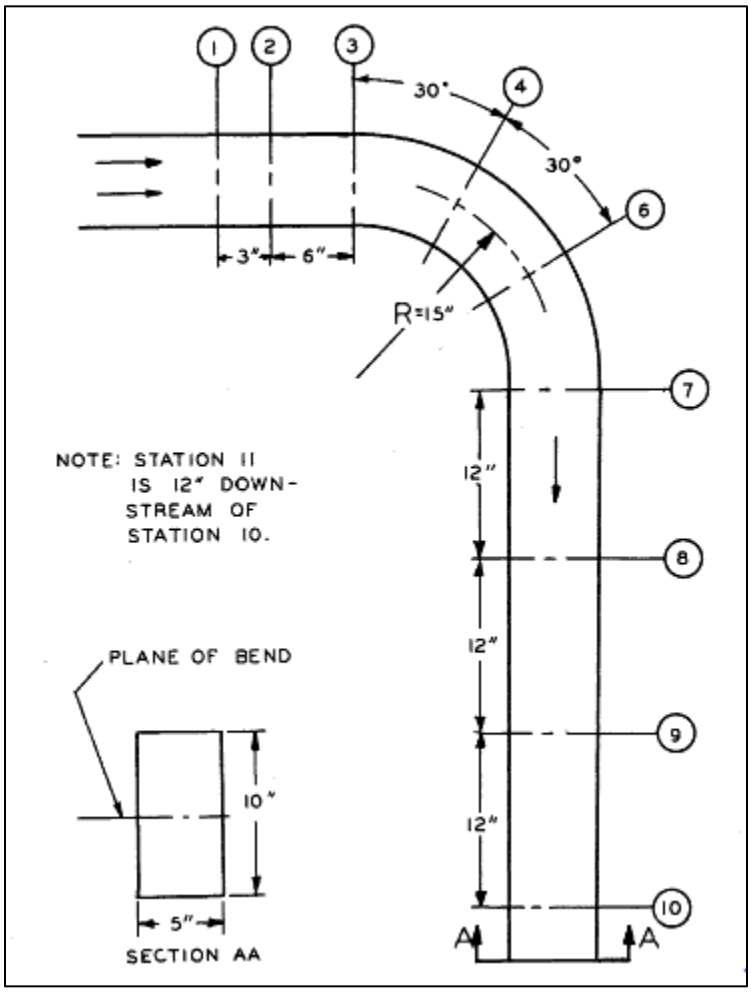

Figure 17: Joy's [4] 90 degree rectangular cross sectional bend with a 15 in. radius experimental configuration.

The stations indicted in the Figure 17 are where velocity measurements were taken to analyze the flow going through the duct. Inlet flow conditions were 85 feet per second. The flow started upstream far enough to have fully developed flow once the flow reached the start of the bend (station 3). Joy's experiment was designed to capture the evidence of secondary circulation phenomena that occurs in rectangular cross sectional ducts downstream of bends. The results obtained from Joy's experiment can be seen in Figure 18.

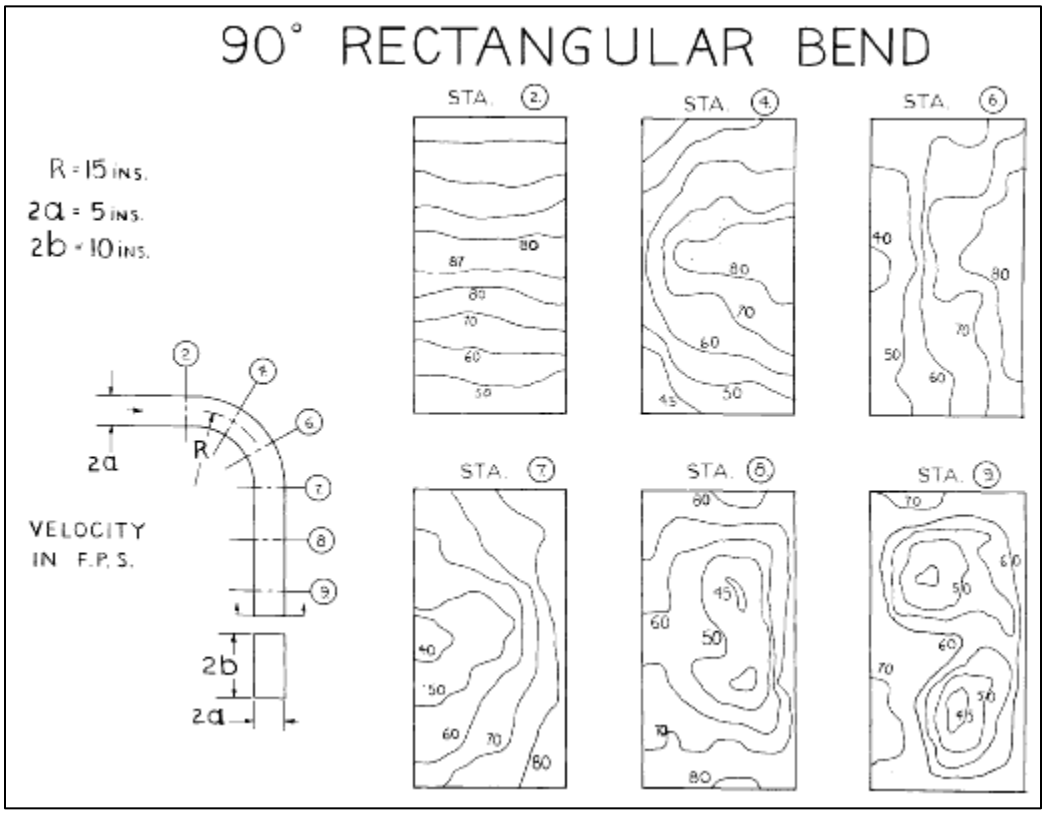

Figure 18: Joy's [4] velocity profiles measured at each marked station.

Station 2 showed that the flow entering the 90 degree bend was fully developed. Station 4 showed the flow starting to hit the outer bend wall, leaving the inner bend corners to have slower velocity profiles. As the flow reaches station 6, the start of a separation bubble on the inner bend wall was developing. At the end of the 90 degree bend at station 7, the separation bubble on the

inner bend wall was more apparent and the faster velocity profile started to separate at the outer bend wall. Station 8 showed the velocity profile starting to swirl displaying some evidence of secondary circulation. The final station (station 9), 24 inches downstream from the end of the 90 degree bend, showed full evidence of secondary circulation which is displayed as two vortices in the duct cross section.

A preliminary geometry was created to simulate Joy's structure he created for his experiment, which can be seen in Figure 19. The geometry created had a 90 degree bend, a square cross section of 5 by 5 inches, and a bend radius of 35 inches. The inlet conditions were: Mach=0.3; ρ_o=0.65288 kg/m^3; T_o=249.15K; μ=1.79x10^{-5}; κ=2.6x10^{-2}; γ=1.4; Re = 2.852x10^7. The grid size was 9,471 points in the flow passage using 78 terms (between 5th and 6th order) for each flow state (density, fluidic velocities (u,v,w), and temperature).

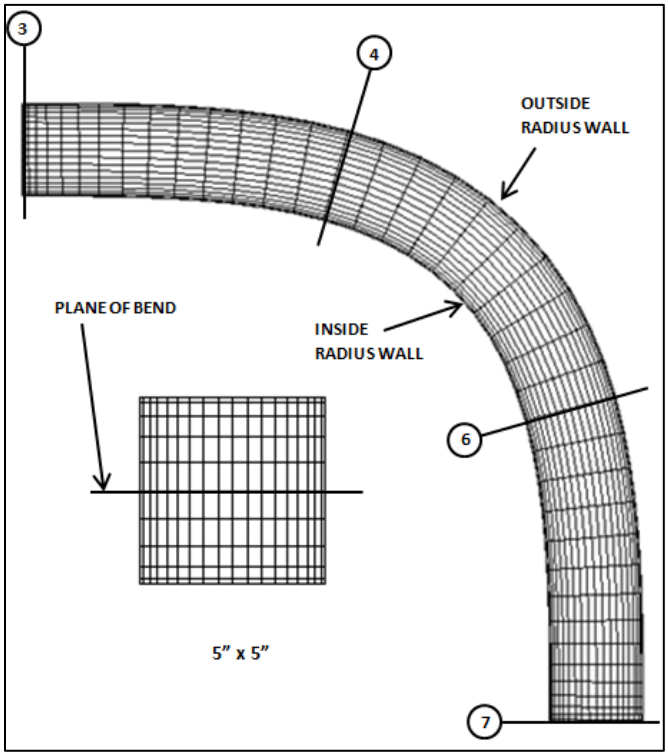

Figure 19: 90 degree square cross sectional bend created to analyze with the spectral methods.

Figure 20 shows the velocity maps of the 3D NS5 solution velocity map predictions. The stations indicated correspond to the same locations in Joy's structure and in the created bend geometry. Although Joy's structure and the created bend geometry are slightly different, both show the formation of the separation bubble and the existence of secondary circulation due to air being forced around a bend. Station 4 shows the formation of the separation bubble on the inner bend radius wall. Station 6 shows the complete separation bubble as well as the introduction of secondary circulation. The virtual air flow hit the outer bend radius wall and was forced to circulate along the outer dimensions of the geometry. Station 8 shows the two vortices that developed due to the secondary circulation. These results directly correspond to Joy's results in showing the existence of a separation bubble as air is forced around a bend as well as the formation of secondary circulation due to a bend. This further verifies the effectiveness and accuracy of the spectral methods and theory described.

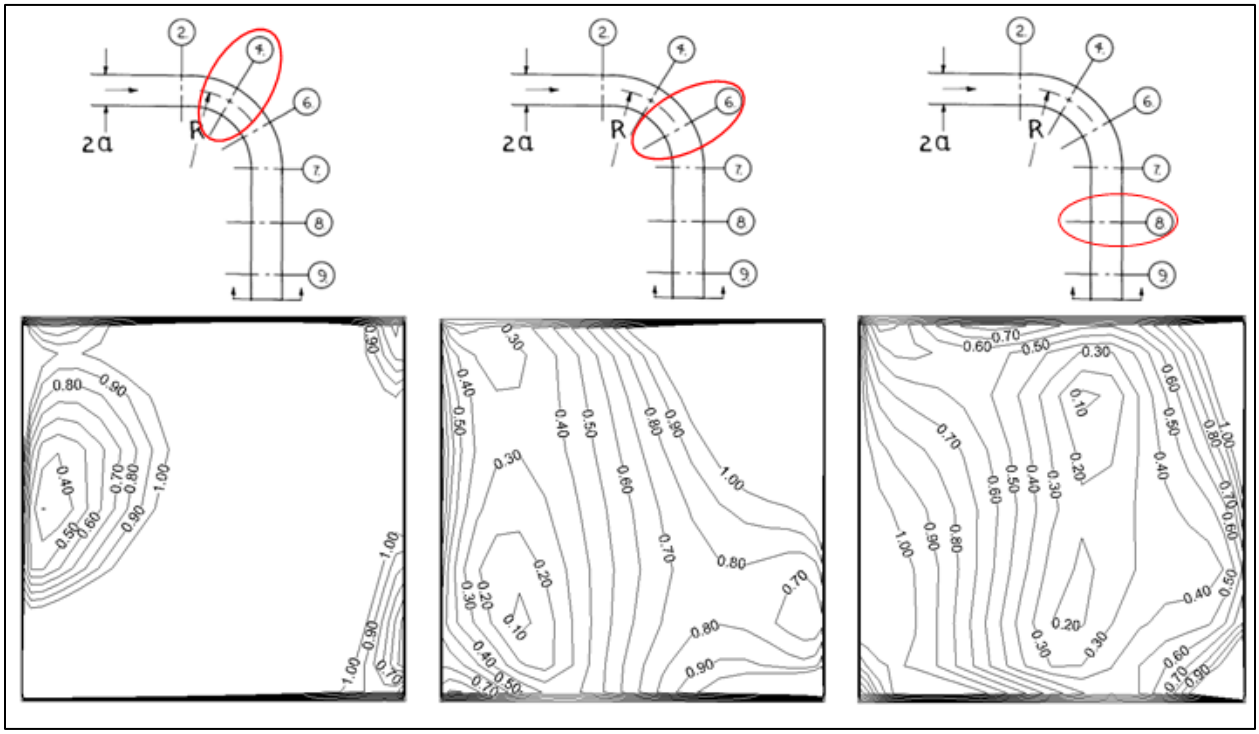

Figure 20: Axial velocity cross sectional contours of the 90 degree square cross sectional bend showing the formation of a separation bubble and the existence of secondary circulation development.

To further verify the solutions obtained from the 90 degree square cross sectional bend problem, the system's Dean Number, Du, was used (Equation 14). The Dean Number is essentially the Reynolds and curvature effects of the system. The y-axis on the plot denotes Reynolds number multiplied by the friction coefficient which is essentially system pressure losses. The Dean number of the system was compared to White's [5] and Collins & Dennis [6] empirical equations for laminar fully developed curve flow, and it was compared to Dean's [7] empirical data for laminar fully developed curve flow (Figure 21). Dean's empirical data had a low Reynolds which corresponds to a lower Dean number whereas the created 90 degree square cross sectional bend had a much larger Reynolds and Dean number. As seen in Figure 21, the 3D spectral solutions matched Collins and Dennis empirical equation (Du > 10^3). At larger Dean Numbers, the pressure losses increase because the flow becomes turbulent where larger pressure losses exist. With a Reynolds number, Re = 2.85x10^7, the flow was turbulent resulting in larger pressure losses.

Dean Number

$$D_u = Re\sqrt{\frac{D_E}{R_c}} \tag{14}$$

where: $D_E = equivalence\ diameter = \frac{4 \times cross\ sectional\ area}{cross\ sectional\ area\ perimeter}$

$$R_c = radius\ of\ curvature = 35\ in$$

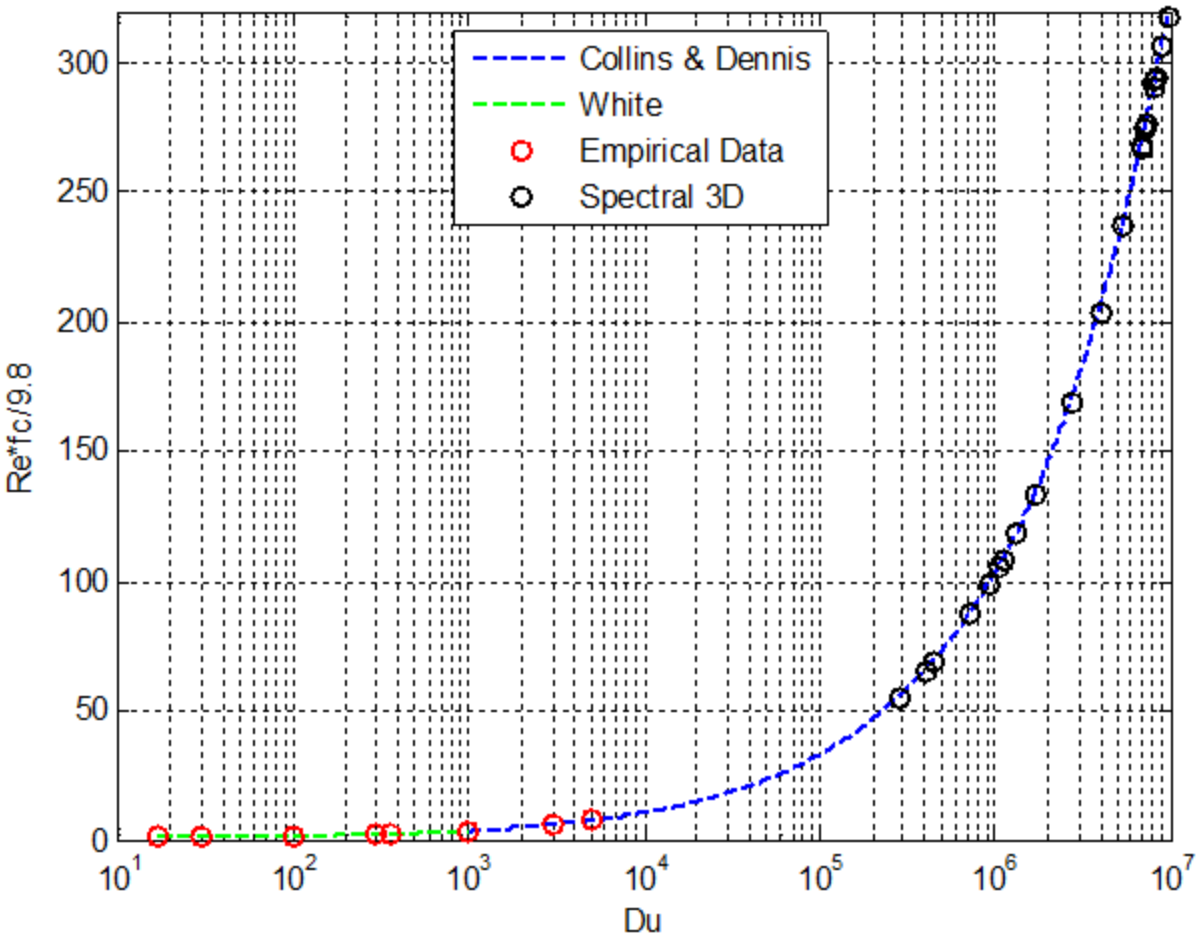

Figure 21: Comparison of pressure loss versus Reynolds curvature effect of experimental results of White's [5], Collins and Dennis [6], and Dean's [7] empirical equations for laminar fully developed curved flow.

Furthermore, the 3D spectral solutions for the 90 degree square cross sectional bend problem was matched against Ito's [8] [9] empirical equation for turbulent flow in rectangular bends (Figure 22). The plot is a comparison of the scaled pressure loss versus the scaled Reynolds curvature effects. As seen from the plot, 3D spectral solutions for the bend problem examined, showed the same form as Ito's equation as if it were an extension to the equation (higher scaled Reynolds curvature effects). The bend problem examined had turbulent flow present due to the large inlet velocity introduced into the bend. The relationships highlighted in Figure 21Figure 22 shows that the 3D spectral solutions obtained are correct solutions for the 90

degree square cross sectional bend problem. The solutions satisfied the empirical equations for laminar fully developed curved flow and for turbulent flow in rectangular bends.

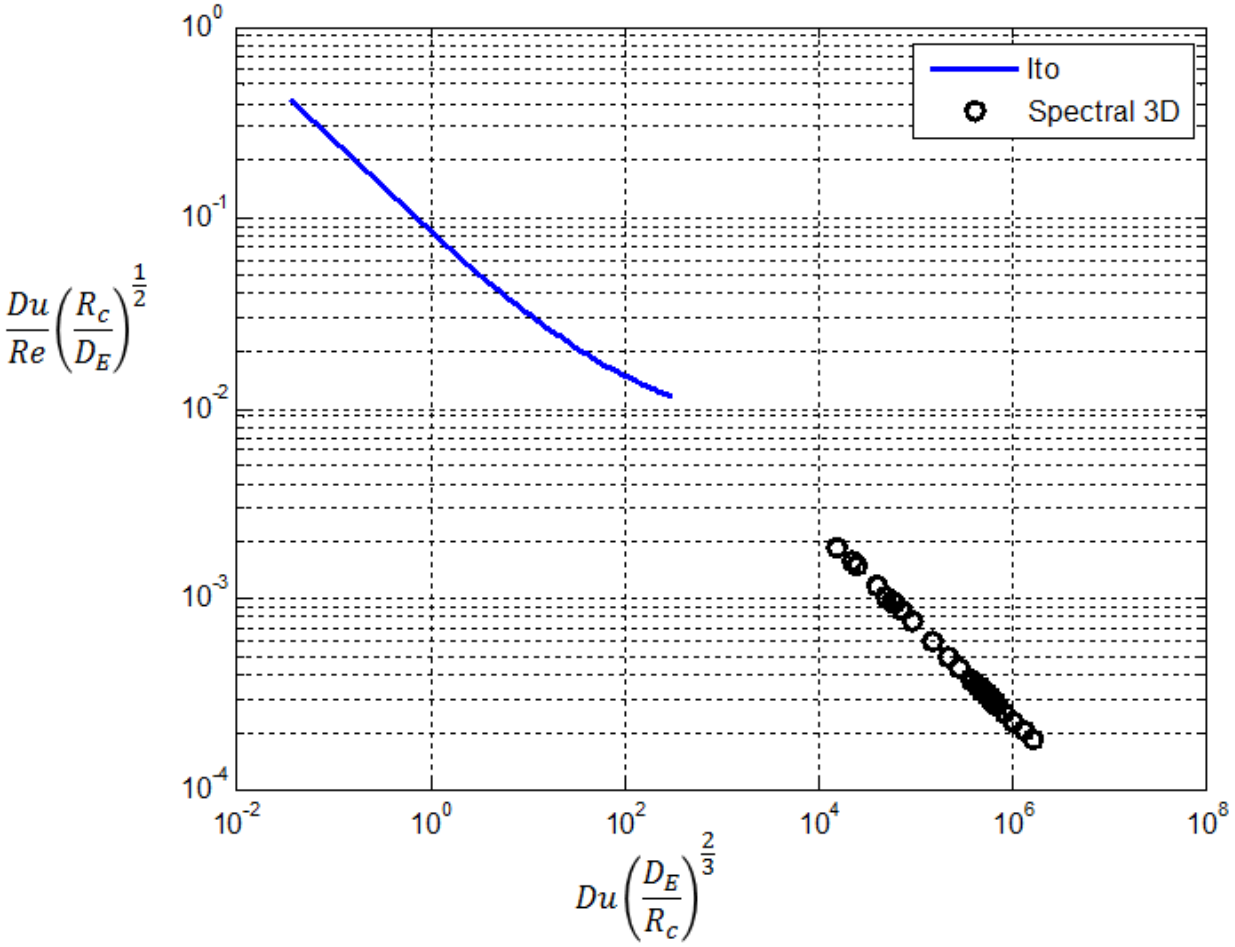

Figure 22: Comparison of scaled pressure loss versus scaled Reynolds curvature effects of experimental results of Ito's [9] [8] empirical equations for turbulent flow in rectangular bends.

Chapter 3: Conclusion and Future Work

After taking a step back and analyzing the three problems mentioned in this thesis, the converging-diverging nozzle, the venturi tube industry nozzle, and the rectangular 90-degree bend duct, the ROM analysis developed has been verified to be working effectively and accurately in obtaining close-form solutions to steady advection-diffusion, unsteady convection-diffusion, and unsteady compressible viscous flow problems. The three problems were chosen specifically to analyze different geometry affects that when combined are similar to turbomachinery problems. One flow domain between a set of rotor blades is very similar to a converging-diverging nozzle problem along with a bend problem. The developed ROM analysis obtained correct solutions for these problems; therefore it can be used for turbomachinery applications.

Future work would entail analyzing NASA test rotor 67 along with other NASA test rotors, standard configuration rotors, and other multistage rotor/stator turbomachines that have experimental test data available to the science community. If the ROM analysis proves to be effective and efficient in obtaining accurate results to turbomachinery problems, it can become a powerful tool that can help the aerospace industry in analyzing jet engines. Loss mechanisms will be predicted inside a jet engine before the engine is even made, which will help engineers and scientists develop better and more advanced jet engines.

Spectral technologies are not a new analysis that is going to replace conventional CFD methodologies, but another analysis that will complement conventional CFD methodologies in analyzing turbomachinery. More research needs to be performed on spectral technologies to catch up with conventional CFD methodologies to prove to be useful along with conventional

CFD methodologies. The future of CFD may involve some type of combination of spectral technologies with conventional CFD methodologies. Only time will tell.

References

[1] R. V. Chima, "Viscous Three-dimensional Calculationss of Transonic Fan Performance," in *CFD Techniques for Propulsion Applications, AGARD Conference Proceedings No. CP-510*, Neuilly-Sur-Seine, France, 1992.

[2] J. E. A. John, Gas Dynamics, 2nd ed. Prentice Hall, Englewood Cliffs, NJ, 1984.

[3] P. Hanley, "A Strategy for the Efficient Simulation of Viscous Compressible Flows using a Multi-domain Pseudospectral Method," *Journal of Computational Physics*, vol. 108, pp. 153-158, September 1993.

[4] W. Joy, Experimental Investigation of Shear FLow in Rectangular Bends, MIT Master's Thesis, 1950.

[5] C. M. White, "Streamline Flow Through Curved Pipes," *Proc. Royal Society A, 123*, pp. 645-663, 1929.

[6] W. N. Collins, "The Steady Motion of a Viscous Fluid in a Curved Tube," *Quart J. Mech. Appl. Math*, vol. 28, no. 2, pp. 133-156, 1975.

[7] W. R. Dean, "Note on the Motion of Fluids in a Curved Pipe," *Phil. Mag. Ser. 7*, vol. 4, no. 20, pp. 208-223, 1927.

[8] H. Ito, "Theory on Laminar Flows through Curved Pipes, Elliptic and Rectangular Cross Sections," *High Speed Mech. Tohoku University, Japan 1*, pp. 1-16, 1951.

[9] H. Ito, "Friction Factor for Turbulent Flows in Curved Pipes," *Trans. ASME, Ser. D, 81*, pp. 123-134, 1959.

Appendix A: Converging-Diverging Nozzle

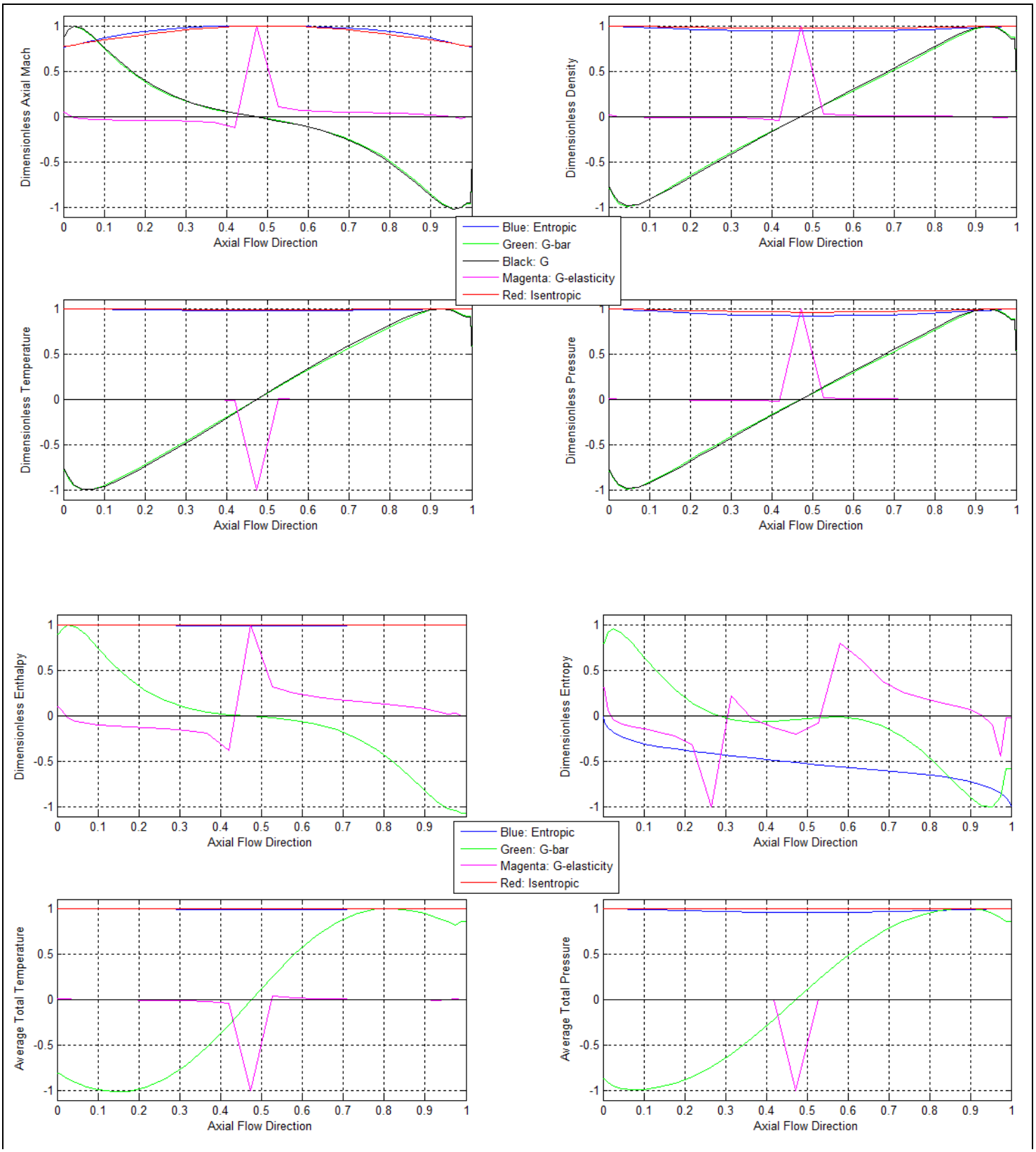

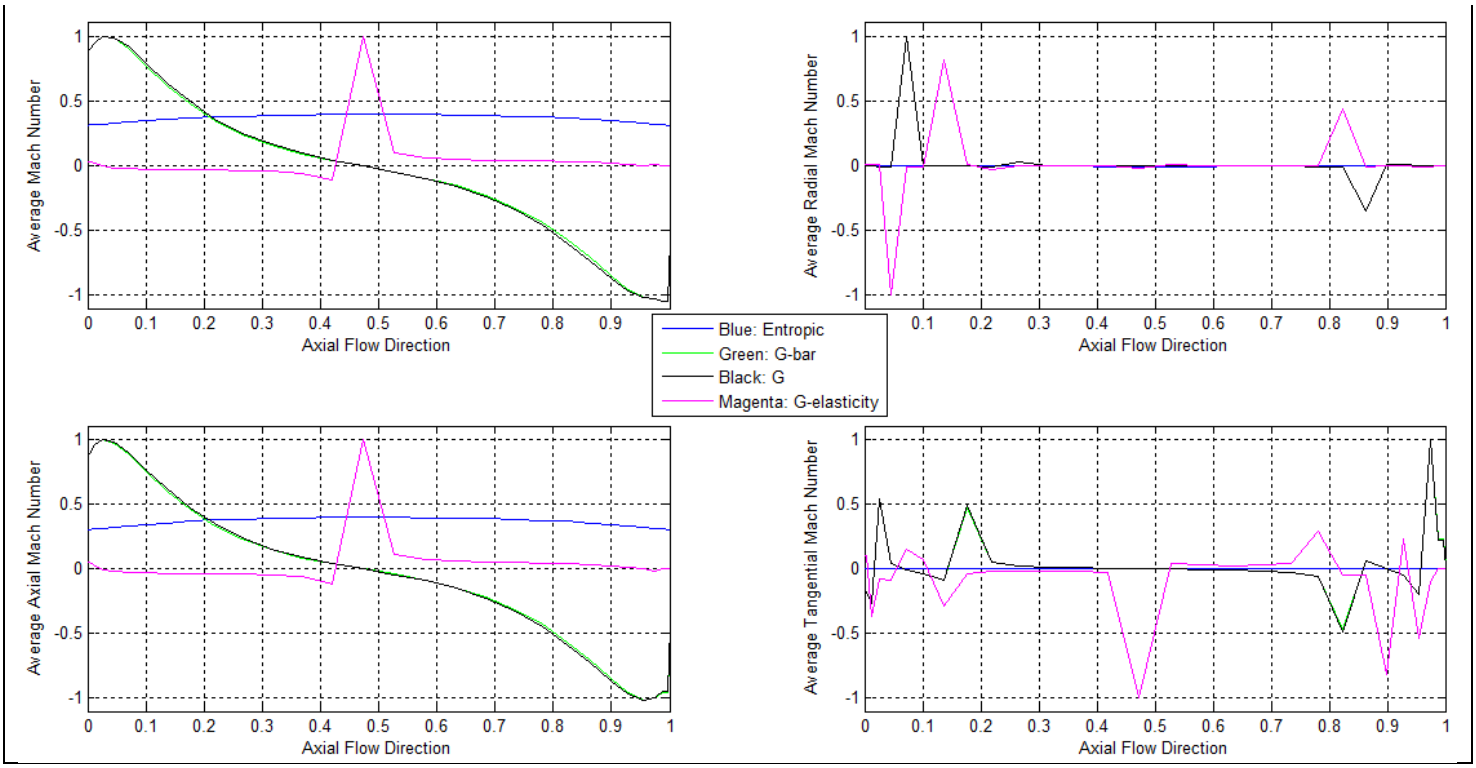

Figure A1: Results of 3D NS5 steady-state conservative subsonic flow solutions computed along with the sensitivities using Chebyshev non-periodic spectral approximations using 286 terms for each flow state (density, fluidic velocity (u,v,w), and temperature) incorporating 27,000 points in passage. Results are normalized to the maximum non-dimensional values of the 3D NS5 solutions.

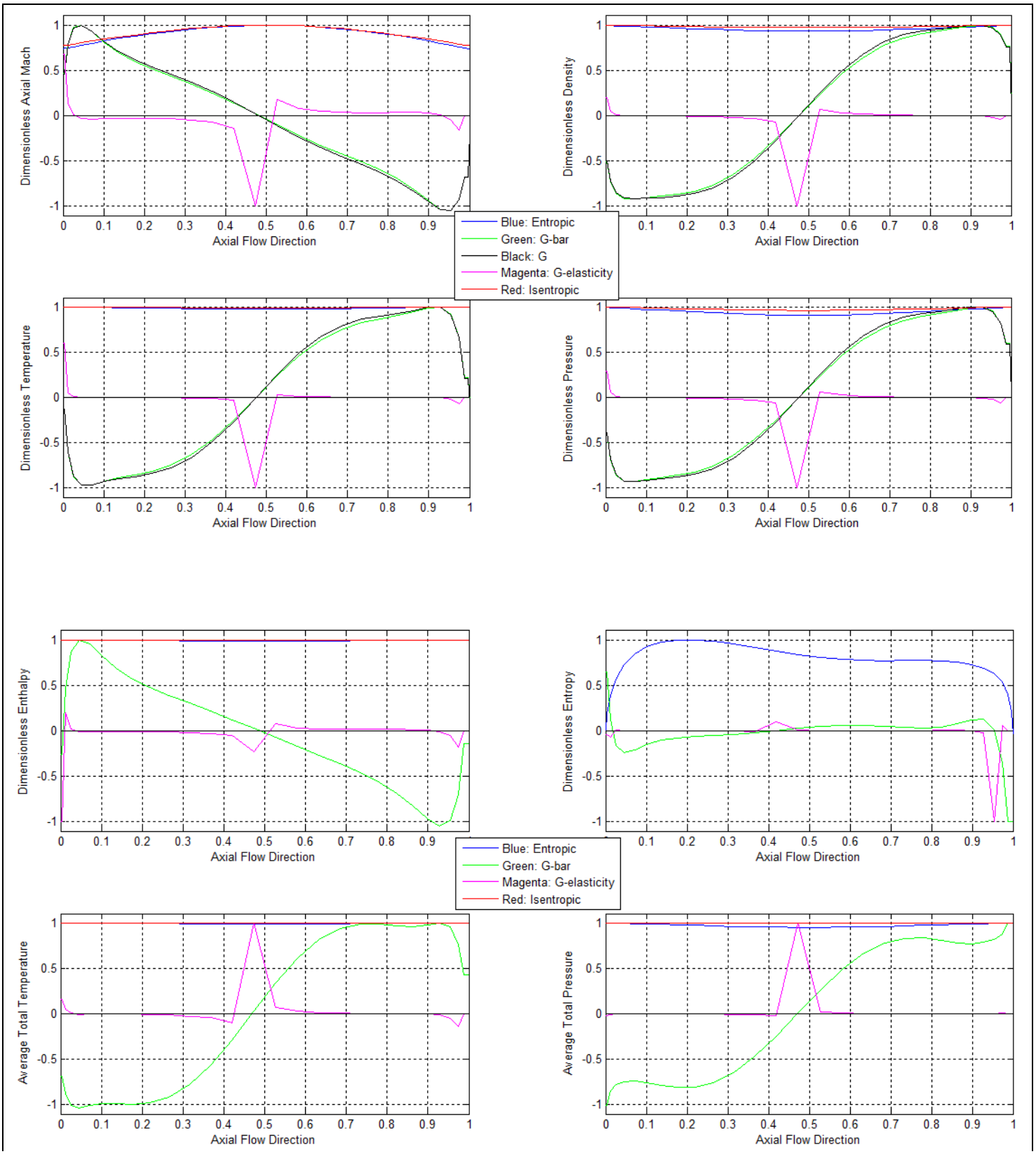
Dimensionless Axial Mach
Axial Flow Direction
Dimensionless Density
Axial Flow Direction
Blue: Entropic
Green: G-bar
Black: G
Magenta: G-elasticity
Red: Isentropic
Dimensionless Temperature
Axial Flow Direction
Dimensionless Pressure
Axial Flow Direction
Dimensionless Enthalpy
Axial Flow Direction
Dimensionless Entropy
Axial Flow Direction
Blue: Entropic
Green: G-bar
Magenta: G-elasticity
Red: Isentropic
Average Total Temperature
Axial Flow Direction
Average Total Pressure
Axial Flow Direction

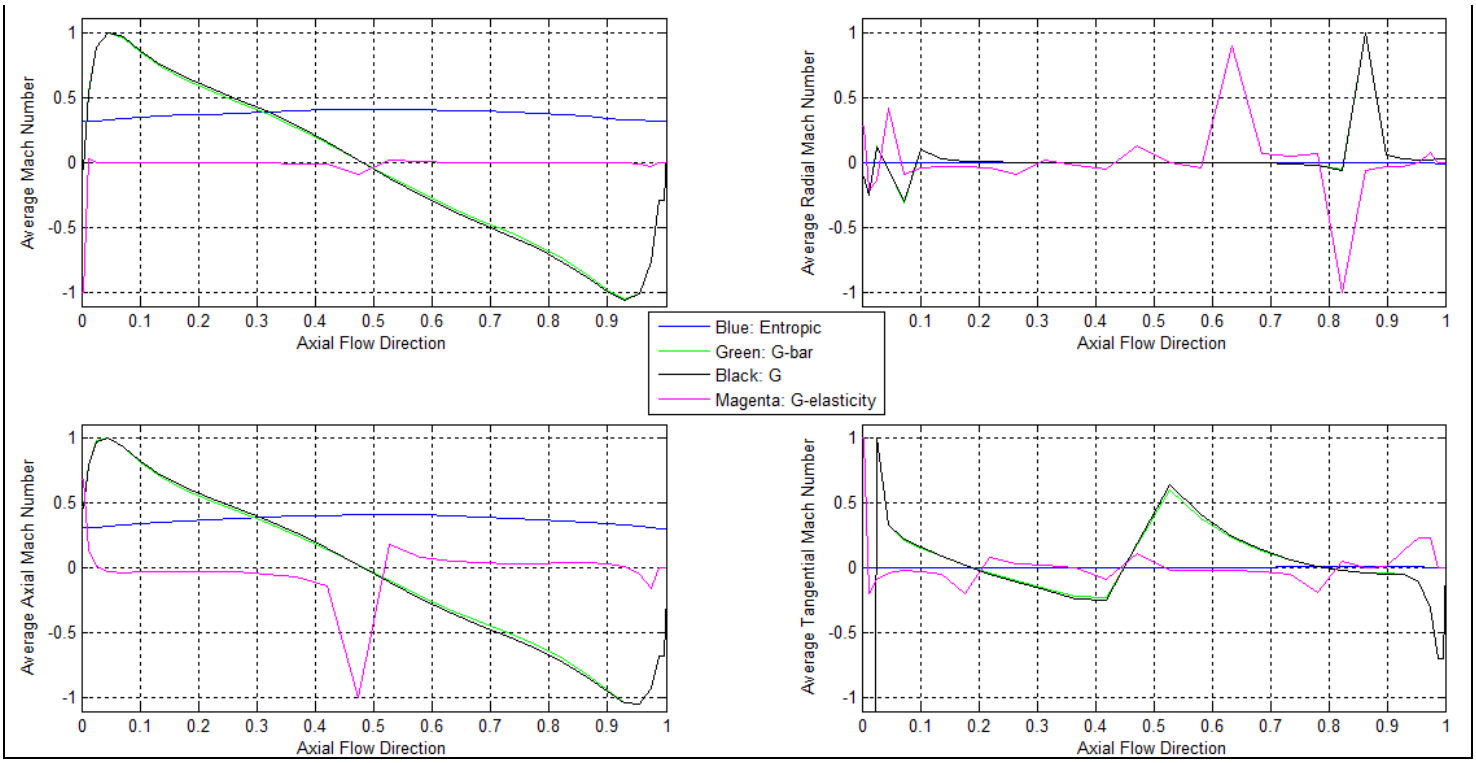

Figure A2: Results of 3D NS5 steady-state conservative subsonic flow solutions computed along with the sensitivities using Chebyshev non-periodic spectral approximations using 455 terms for each flow state (density, fluidic velocity (u,v,w), and temperature) incorporating 27,000 points in passage. Results are normalized to the maximum non-dimensional values of the 3D NS5 solutions.

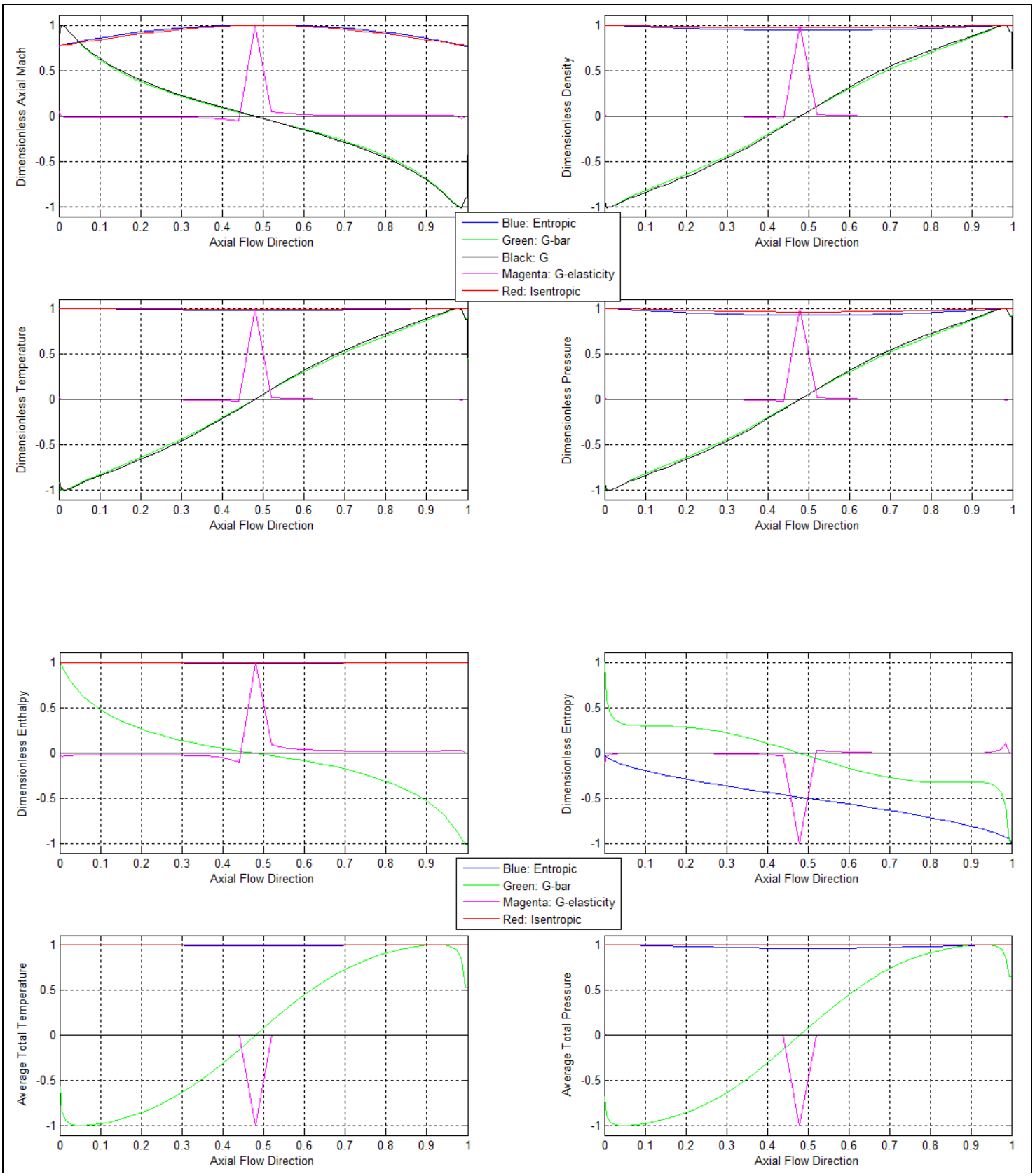
Dimensionless Axial Mach
Dimensionless Density
Dimensionless Temperature
Dimensionless Pressure
Dimensionless Enthalpy
Dimensionless Entropy
Average Total Temperature
Average Total Pressure
Axial Flow Direction
Blue: Entropic
Green: G-bar
Black: G
Magenta: G-elasticity
Red: Isentropic

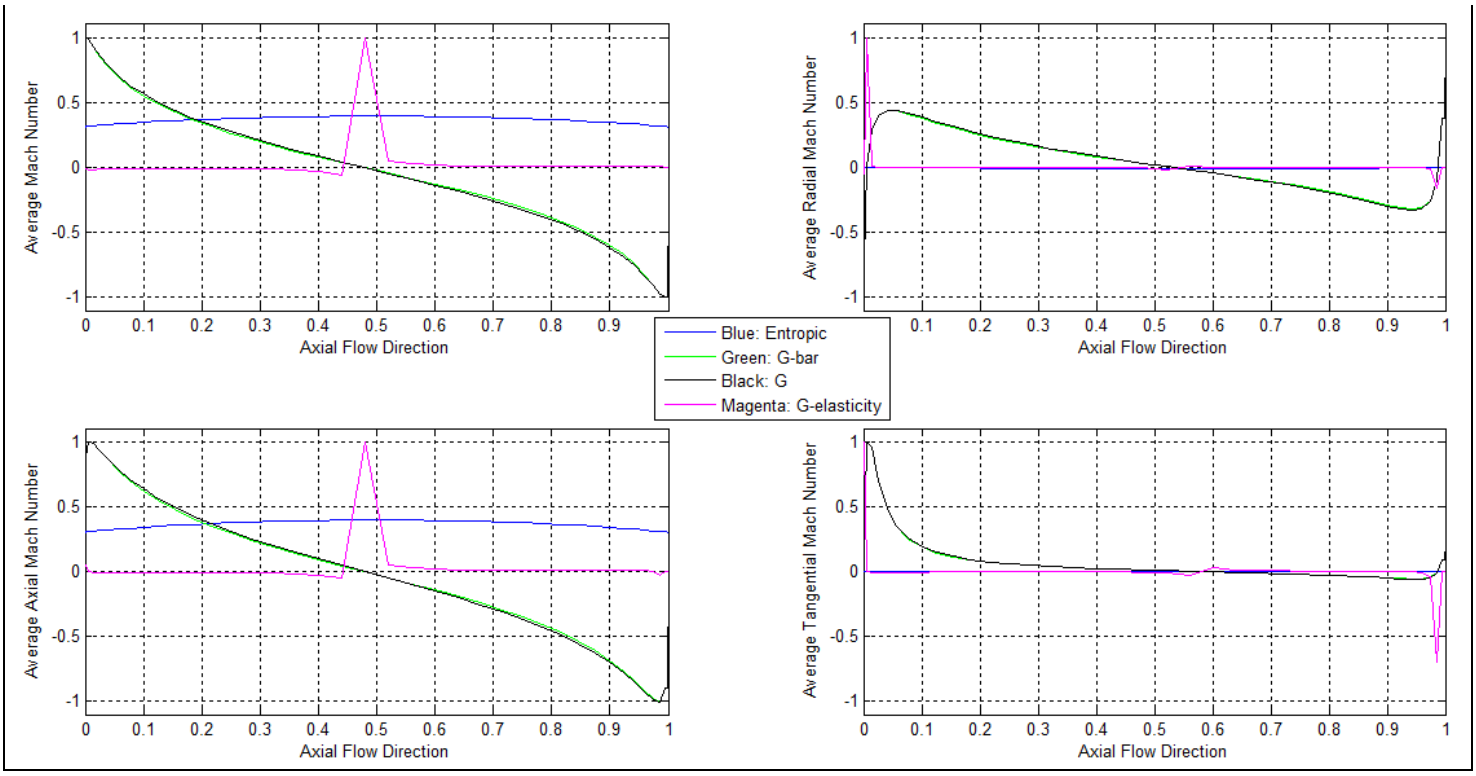

Figure A3: Results of 3D NS5 steady-state conservative subsonic flow solutions computed along with the sensitivities using Chebyshev non-periodic spectral approximations using 35 terms for each flow state (density, fluidic velocity (u,v,w), and temperature) incorporating 64,000 points in passage. Results are normalized to the maximum non-dimensional values of the 3D NS5 solutions.

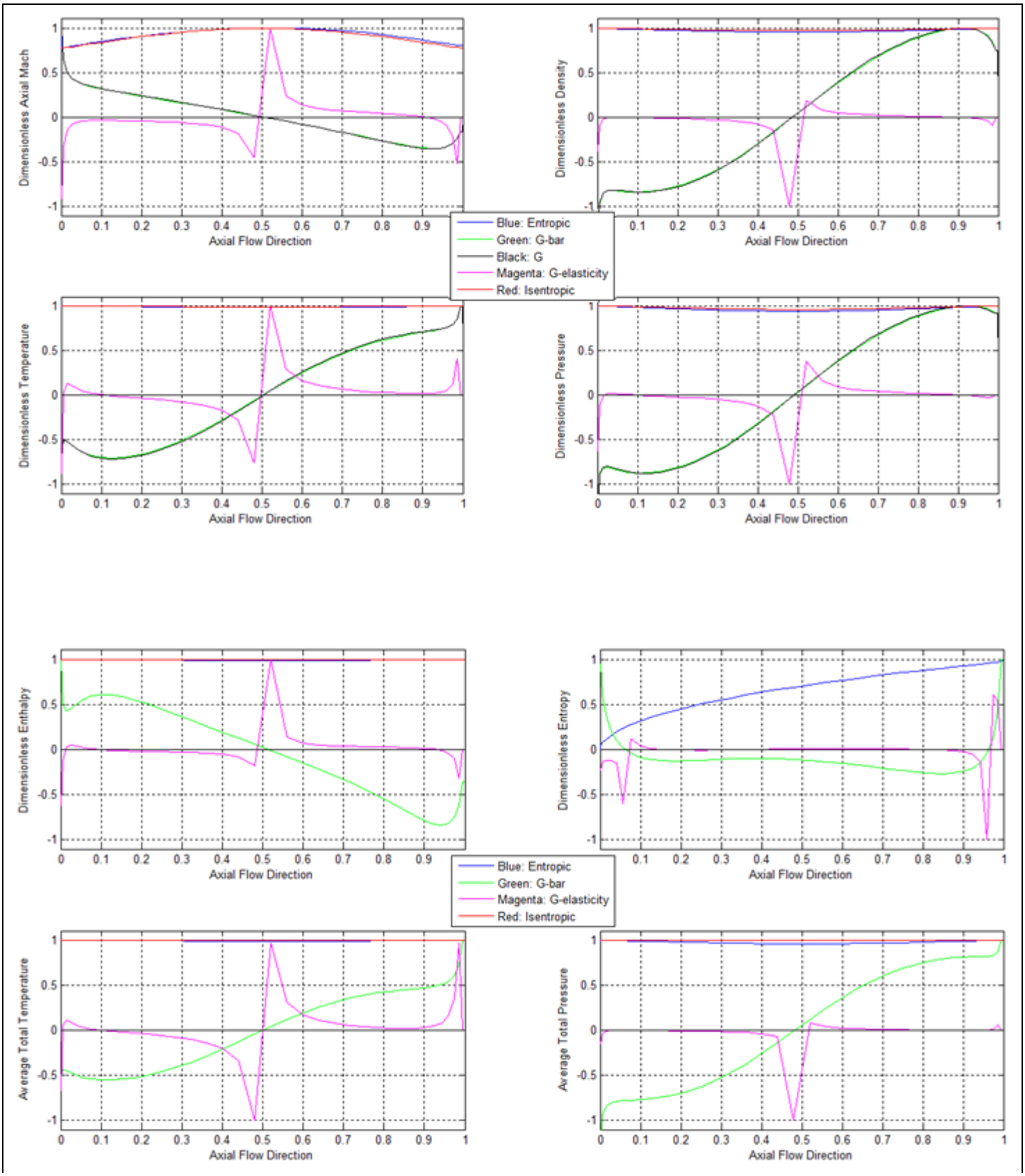
Dimensionless Axial Mach
Dimensionless Density
Dimensionless Temperature
Dimensionless Pressure
Axial Flow Direction
Blue: Entropic
Green: G-bar
Black: G
Magenta: G-elasticity
Red: Isentropic
Dimensionless Enthalpy
Dimensionless Entropy
Average Total Temperature
Average Total Pressure

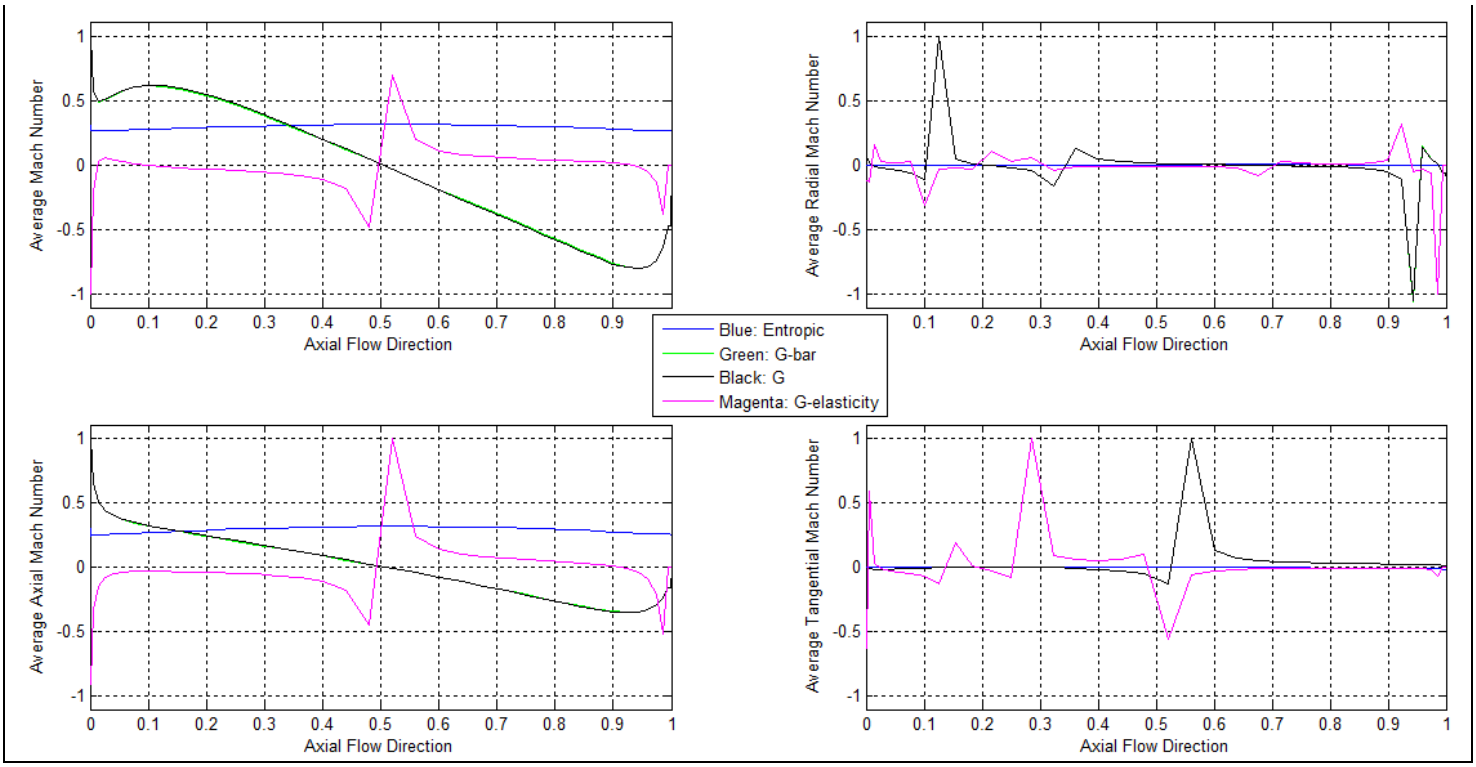

Figure A4: Results of 3D NS5 steady-state conservative subsonic flow solutions computed along with the sensitivities using Chebyshev non-periodic spectral approximations using 120 terms for each flow state (density, fluidic velocity (u,v,w), and temperature) incorporating 64,000 points in passage. Results are normalized to the maximum non-dimensional values of the 3D NS5 solutions.

Appendix B: Venturi Tube Industry Nozzle

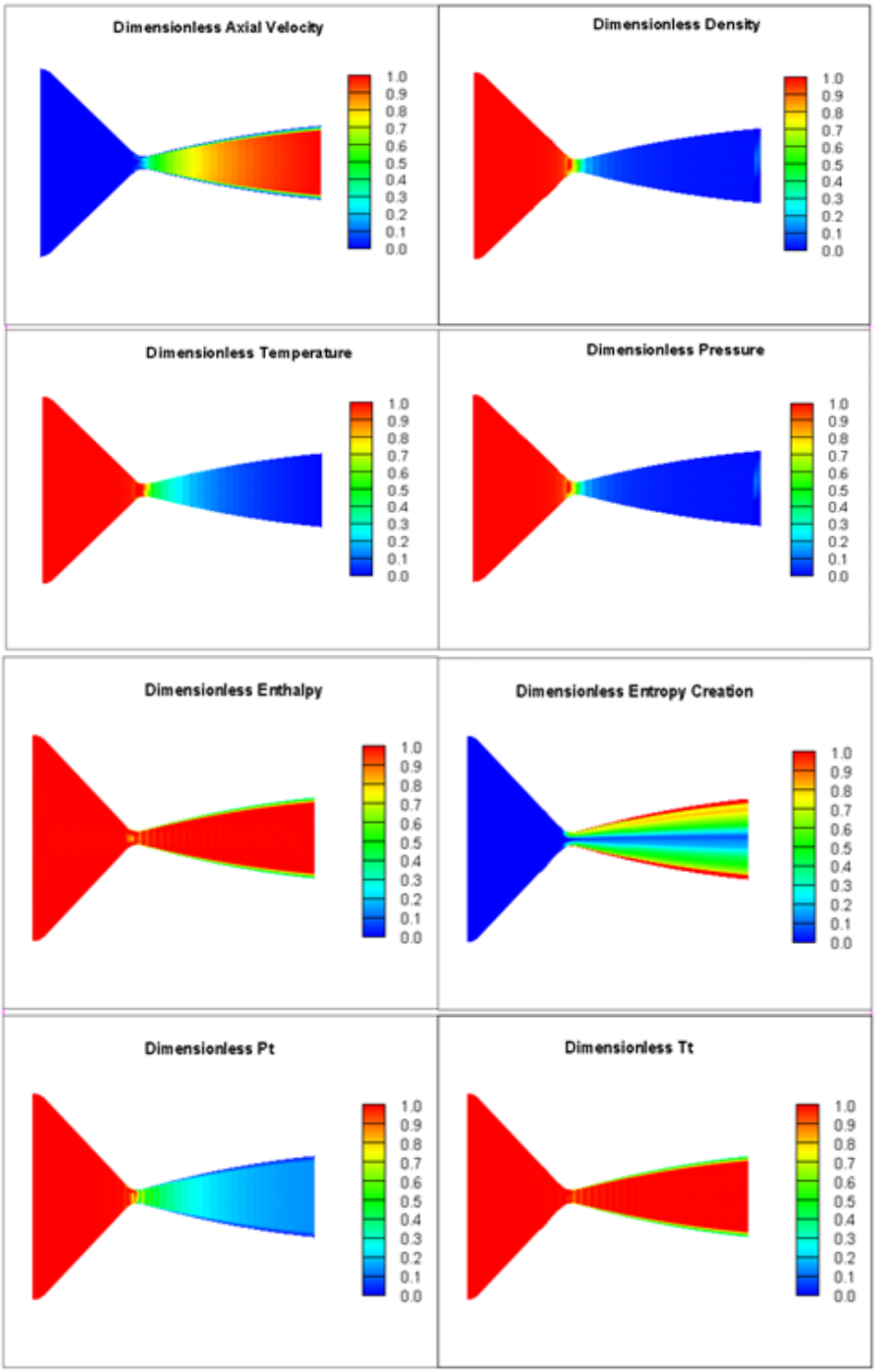

Figure B1: Contours of transonic and supersonic transport non-dimensional flow properties (axial Mach, density, temperature, pressure, enthalpy, entropy creation, stagnation pressure, and stagnation temperature) across a gradually converging-diverging industry nozzle, 3-D NS5 steady-state solutions, assuming $M_{throat} = 1$, results obtained using Legendre non-periodic spectral approximations, 600 total terms (NS5 solutions), each involving 164,000 points in 41 sub-domains.

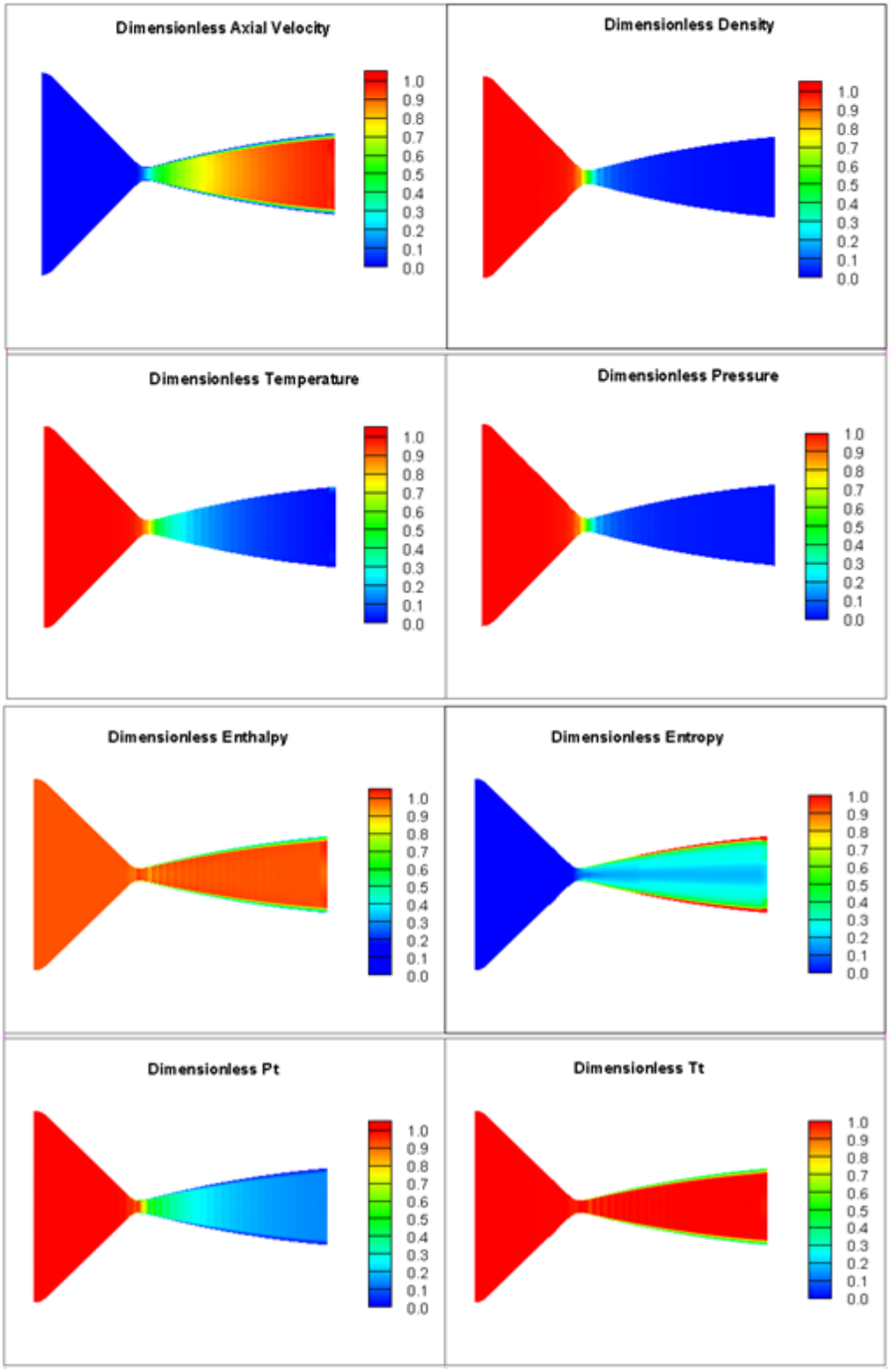

Figure B2: Contours of transonic and supersonic transport non-dimensional flow properties (axial Mach, density, temperature, pressure, enthalpy, entropy creation, stagnation pressure, and stagnation temperature) across a gradually converging-diverging industry nozzle, and 3-D NS8 steady-state solutions, assuming M_{throat}= 1, results obtained using Legendre non-periodic spectral approximations, 960 total terms (NS8 solutions), each involving 164,000 points in 41 sub-domains.